

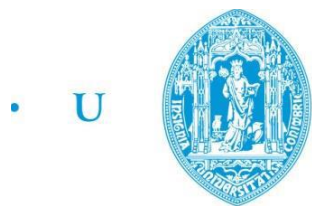
Khawaja Khalid Raza

Effect of grooved surface texturing on the behavior of lubricated contacts

Submitted in partial fulfillment of the requirements for the degree of Masters in Tribology of Surface and Interfaces
2016



UNIVERSIDADE DE COIMBRA



• U • C •

FCTUC

FACULDADE DE CIÊNCIAS
E TECNOLOGIA
UNIVERSIDADE DE COIMBRA

Influência da texturização superficial no comportamento de contactos lubrificados

Effect of grooved surface texturing on the behavior of lubricated contacts

Submitted in Partial Fulfilment of the Requirements for the Joint European Master in tribology of Surfaces and Interfaces

Author: Khawaja Khalid Raza

Supervisors:

Amílcar Ramalho, Associated Professor at University of Coimbra

Luis Vilhena, Researcher at University of Coimbra

Jury:

Bruno Trindade, Associated Professor at University of Coimbra

Stephen Muhl, Researcher at University of Mexico

Paulo Ferreira, Full Professor at University of Austin (USA)



Coimbra, July, 2016

Acknowledgement

First, I am heartily thankful to my Supervisors Professor Amílcar Ramalho and Dr. Luis Vilhena whose encouragement, guidance and support from the initial to the final level enabled me to develop an understanding of this work. This work couldn't be completed without the effort and co-operation of Dr. Luis Vilhena. His contributions are sincerely appreciated and gratefully acknowledged. I would also like to take this opportunity to thank my teacher, Professor Albano Cavaleiro for his guidance. Many thanks for TRIBOS Consortium who selected me in this prestigious program. I pay my special thanks to all Professors, lecturers and Colleagues whose knowledge and support help me completion of this master's program. I would like to thank my teacher Mr. Bilal Saleem who introduced me about tribology. Above all, to the great Almighty God, who is author of all knowledge's and wisdoms.

LIST OF FIGURES

Figure 2.1. Segments of piston rings.....	8
Figure 2.2. A view of pores on the SiC ring (magnification x25).....	10
Figure 3.1. The hydrodynamic effect of the single idealized dimple.....	11
Figure 3.2. (a) Schematic of a computational cell with a moving smooth wall against a stationary textured wall with inlet textures, showing key geometry. (b) Prediction for pressure on top wall.....	12
Figure 3.3. The Spatial Texture Density (D/L) for 2D Textured Model.....	13
Figure 3.4. The Coefficient of Friction vs. the Spatial Texture Density (D /L).....	14
Figure 3.5. Stribeck curves showing modes of lubrication.....	17
Figure 3.6. The Stribeck curves of the ground, polished and dimpled (textured).....	18
Figure 3.7. Effect of shape and orientation of texture on friction.....	22
Figure 3.8. Summary of the performance of the textured surfaces in starved boundary lubricated sliding.....	23
Figure 3.9. Effect of viscosity on Stribeck Curve.....	24
Figure 4.1. Pattern geometry and dimensions.....	28
Figure 4.2. Micrographs of surface textured patterns: (a) textured with low density-TLowD textured with medium density-TMediumD and, (c) textured with high density-THighD.....	29
Figure 4.3. 2D profile of TLowD specimen illustrating the shape and dimensions of typical micro-grooves.....	30
Figure 4.4. Roughness profile (single cone).....	30
Figure 4.5. Block on ring sliding test tribometer used for testing.....	31
Figure 4.6. Schematic diagram of the block-on-ring sliding test tribometer.....	33
Figure 5.1. Variation in coefficient of friction with sliding speed for un-textured and textured surfaces lubricated with ISO VG 40: $\nu_{40} = 46.8 \text{ mm}^2/\text{s}$ and at 40 N applied load.....	35
Figure 5.2. Variation in coefficient of friction with sliding speed for un-textured and textured surfaces lubricated with ISO VG 320: $\nu_{40} = 320 \text{ mm}^2/\text{s}$ ($F_N = 40 \text{ N}$).....	36
Figure 5.3. Variation in coefficient of friction with sliding speed for un-textured and textured surfaces lubricated with ISO VG 150: $\nu_{40} = 150 \text{ mm}^2/\text{s}$ ($F_N = 40 \text{ N}$).....	37

Figure 5.4. Variation in coefficient of friction with sliding speed for un-textured and textured surfaces lubricated with ISO VG 40: $\nu_{40} = 46.8 \text{ mm}^2/\text{s}$ and ISO VG 320: $\nu_{40} = 320 \text{ mm}^2/\text{s}$ ($F_N = 40 \text{ N}$).....38

Figure 5.5. Variation in coefficient of friction with sliding speed for un-textured and textured surfaces lubricated with ISO VG 40: $\nu_{40} = 46.8 \text{ mm}^2/\text{s}$ and ISO VG 150: $\nu_{40} = 150 \text{ mm}^2/\text{s}$ ($F_N = 40 \text{ N}$).....40

Figure 5.6. Variation in coefficient of friction with sliding speed for un-textured surfaces lubricated with ISO VG 40: $\nu_{40} = 46.8 \text{ mm}^2/\text{s}$ (PAO8), ISO VG 150: $\nu_{40} = 150 \text{ mm}^2/\text{s}$ and ISO VG 320: $\nu_{40} = 320 \text{ mm}^2/\text{s}$ ($F_N = 40 \text{ N}$).....41

Figure 5.7. Variation in coefficient of friction for textured and un-textured surfaces lubricated with ISO VG 40: $\nu_{40} = 46.8 \text{ mm}^2/\text{s}$ (PAO8), ISO VG 150: $\nu_{40} = 150 \text{ mm}^2/\text{s}$ and ISO VG 320: $\nu_{40} = 320 \text{ mm}^2/\text{s}$ ($F_N = 40 \text{ N}$).....42

Figure 5.8. Average Stribeck curves for textured and un-textured surfaces lubricated with ISO VG 40: $\nu_{40} = 46.8 \text{ mm}^2/\text{s}$ (PAO8), ISO VG 150: $\nu_{40} = 150 \text{ mm}^2/\text{s}$ and ISO VG 320: $\nu_{40} = 320 \text{ mm}^2/\text{s}$ ($F_N = 40 \text{ N}$).....43

LIST OF TABLES

Table 3.1. Operating film thickness, Coefficient of friction and wear for various lubrication modes.....	16
Table 3.2. Summary of literature in the experimental domain and the key parameters studied..	19
Table 3.3. Summary of literature in the numerical domain and the key parameters studied... ..	20
Table 3.4. Features of surface texture.....	21
Table 4.1. Steel chemical composition in weight %.....	27
Table 4.2. Main features characteristics of the textured disc patterns.....	29
Table 4.3. Lubricant properties.....	33
Table 5.1. Specific film thickness (λ) values for six different sliding speeds and three different lubricant viscosities, showing the variation in the lubrication regime (boundary - light blue: $\lambda < 1$; mixed - blue: $1 < \lambda < 5$ and hydrodynamic - dark blue $\lambda > 5$).....	44

SYMBOLGY AND ACRONYMS

Symbology:

Ap: pattern area density.

B: rhomb width.

t: the groove width.

α : the intersection angle.

Acronyms:

HD: Hydrodynamic lubrication.

EHL: Elasto-hydrodynamic lubrication.

BL: Boundary lubrication.

DLC: Diamond like carbon.

LST: Laser surface texturing.

RIE: Reactive ion etching.

PL: Photolithography.

KOH: Potassium hydroxide.

DRIE: Deep reactive ion etching.

PAG: Polyalkylene glycol.

POE: Polyol ester.

VG: Viscosity grade.

NS: Navier-Stokes.

FT: Film thickness.

Re: Reynolds number.

C/S: cross-section

Soft elasto-hydrodynamic lubrication (SEHL)

Abstract

The goal of this research study was to investigate the effect of grooved surface texturing with a rhombic geometry under different lubrication regimes. Tribological study under unidirectional sliding was focused on the effect of texturing parameters such as groove depth, groove width, distance between grooves and pattern area density on the coefficient of friction under different lubrication regimes achieved by varying sliding speed and lubricant viscosity. Three types of grooved patterns with different textured area densities were produced on steel samples by electrical discharge machining (EDM). The largest gain in terms of friction reduction was observed by using lowest texture density specimen by using medium viscosity oil (ISOVG 150) at higher sliding speeds. Inspection of sliding surfaces has not revealed any measurable wear for the contact conditions investigated.

Keywords: Surface texturing, grooves, block-on-ring, Stribeck curves

Resumo

O objetivo deste estudo foi investigar o efeito de texturização de superfície sulcada com uma geometria rômica sob diferentes regimes de lubrificação. O estudo tribológico sob deslizamento unidirecional foi focado no efeito dos parâmetros de texturização, como a profundidade do canal, largura do canal, distância entre sulcos e densidade de área de padrão sobre o coeficiente de atrito sob diferentes regimes de lubrificação conseguido através da variação da velocidade de deslizamento e viscosidade do lubrificante. Três tipos de padrões sulcados com diferentes densidades de área texturizados foram produzidos em amostras de aço por eletroerosão (EDM). Os resultados desta investigação mostraram que, sob a lubrificação fronteira, as texturas resistem ao deslizamento, assim, resultando em maior atrito. O maior ganho em termos de redução de atrito foi observada sob lubrificação hidrodinâmica. Inspeção das superfícies deslizantes não revelou nenhum desgaste mensurável para as condições de contacto investigados.

Palavras-chave: texturização de superfície, sulcos, calços, no anel, curvas Stribeck

Table of contents

1. Introduction	1
1.1. Objectives	1
1.2. Importance of texturing	1
1.3. Parameters in surface texturing	2
1.4. Methods of texturization	4
1.5. Thesis structure	4
1.5.1. Previous experimental approach	4
1.5.2. New experimental approach	5
1.5.3. Contact geometry	5
1.5.4. Unidirectional test	5
1.5.5. Stribeck curves	6
2. Industrial problems and scope of texturization	7
2.1. Reciprocating automotive components	7
2.2. Automobile engine mechanical components	8
2.2.1. Piston-cylinder system	8
2.2.2. Piston rings	8
2.2.3. Seals, pumps and valves	9
2.2.4. Cylinder liner	9
2.2.5. Mechanical Seals	10
2.2.6. Journal and thrust bearings	10
3. State of art	11
3.1. Basic theory of texturization	11
3.2. Use of dimples for textured surfaces	12
3.3. Spatial texture density	13
3.4. Effect of texturing on Stribeck curves	15
3.4.1. Effects of texture size, shape, area fraction, and orientation	21
3.4.2. Effect of sliding velocity and lubricant viscosity on film thickness	24
4. Materials and Methods	26
4.1. Types of Pattern	27

4.1.1. Specimens	27
4.2. Characterization of samples surface	30
4.3. Calculation of cone area	31
4.4. Experimental procedure	31
5. Results and discussion	34
5.1. Effect of lubricant viscosity and pattern area density on COF	34
5.1.1. ISO VG 46 (PAO8)	34
5.1.2. High viscosity oil – ISO VG 320	35
5.1.3. Medium viscosity oil – ISO VG 150	36
5.2. Comparison between different lubricant viscosities	37
5.2.1. Comparison between low viscosity (ISO VG 46) and high viscosity (ISO VG 320) oil	37
5.2.2. Comparison between low viscosity (ISO VG 46) and medium viscosity (ISO VG 150) oil	39
5.3. Stribeck curves	40
5.4. Effect of sliding velocity and lubricant viscosity on transitions in lubrication regimes	43
6. Conclusions	45
Bibliography	46

1. Introduction

1.1. Objectives

The main purpose of this work was to decrease coefficient of friction and improving wear performance by means of patterning of steel surface. So, the objective was to first investigate effect of incorporating texturing such as grooves on frictional behavior of steel specimen's surface under lubricated conditions. Grooved patterns with different densities were prepared. The goal was to get Stribeck curves by selecting proper experimental conditions like load, speed and viscosity conditions. The literature shows that by using texturing effect surfaces can increase their capacity for higher loads. The reason is that dimples or groove provides reservoir for oil and collecting wear particles from surfaces.

1.2. Importance of texturing

Characteristics of contact surfaces has great influence on tribological behaviour of the contact, including friction and wear, and thus determining energy consumption and system efficiency. Ever increasing demands for capacity and reliability of mechanical systems and especially smaller consumptions of energy, fuels and lubricants, dictate use of new advanced materials and surface technologies, which would increase efficiency and reduce energy consumption and impact on environment. Right tribological characteristics of contact surfaces, being greatly influenced by surface topography, determine the possibility for energy saving and mechanical systems efficiency improvement [1,2].

From a standpoint of reducing energy consumption and increasing systems efficiency, one of the most important surface characteristics is its roughness or topography and its impact on friction and wear. In the field of surface topography and its effect on tribological properties of contact surfaces, a lot of research work has already been done [3-10], which in the case of surface texturing usually doesn't have physical background and doesn't give correlations between texturing parameters and friction. However, research work in the area of surface texturing, the way to modify contact surface through formation of micro-dimples or micro-channels shows that by using suitable structure of micro-dimples and grooves considerable improvement in friction and wear properties of contact surfaces can be expected [2,11-12].

One of the first commercial applications of surface texturing involves honing of cylinder liners in internal combustion engines. One of the leading carmakers succeeded in reducing fuel consumption for 2.5 % by the use of micro-dimples on contact surfaces of engine components [13].

Besides that, surface texturing can be found in the field of magnetic media for storing data, MEMS (micro-electronic mechanical systems) devices, as well as face seals, piston rings, sliding bearings etc. The biggest research, however, was done in the field of sliding bearings and face seals, where laser surface texturing is normally used. [14-15]. In case of hydrodynamic, elasto-hydrodynamic or mixed lubrication, micro-dimples act as micro-hydrodynamic bearings, and in conditions of boundary lubrication as micro-reservoir for lubricant and in conditions of dry sliding as micro-traps for wear particles [16].

Generally, textures fulfill the three major roles depending upon lubrication regime. Firstly, it traps wear debris. Secondly, it acts as lubricant reservoir and finally, it acts as hydrodynamic bearing. The wear debris entrapment is one of major effects in any lubrication regime and in any type of contact. This reduces wear, increases component life and improves fretting fatigue resistance. Textures act like micro reservoirs for boundary and mixed lubrication regimes and provides lubricant during whole operating period [17].

1.3. Parameters in surface texturing

The main parameters in texturing are diameter, depth, shape and density of the structure. Effect of texturing largely depends on operating contact conditions such as sliding speed and contact pressure. Selection of optimal texturing parameters is still based on experimental approach. This is also the main reason for very large variation of texturing parameters, which different authors are describing as optimal. Solutions, which are already in use in practice, are mainly the result of extensive experimental testing and hunting for optimal solution for a given application. Incorporation of solid lubricants on to textured and coated surface too decreases friction coefficient and increases wear resistance [18].

Friction reduction in parts of combustion engines improves efficiency and reduces fuel consumption. Therefore, the various options like improved design of contact surfaces, lubrications, coatings and surface texturing must be used for this purpose. Some texturing

features are discontinuous like dimples and pores while others are continuous like grooves and cross hatched patterns [19].

Various texturing shapes include dimples, grooves, squares, chevrons, ellipses, pyramids. Surface texturing has emerged in surface engineering which significantly improves load capacity, wear resistance and friction coefficient. The load carrying capacity of textured journal bearing increases at constant speed and oil supply with respect to smooth journal bearing. Similarly, the same is the case with increase of maximum pressure while keeping load and oil pressure constant [20].

Texturing changes flow and film thickness of lubricating film across contact region. It also serves as channels to supply lubricant to the surface and alters bearing pressure distribution [21]. Friction relates to asperity shape and slope, asperity shape and slope relates to surface texture. Conventional electrical discharge machining (EDM) can be used for macro- and micro-surface patterning. Conventional electrical discharge machining is based on the evaporation of material by electrical arcs between electrode and machined surface [22]. This work focuses on textured discs produced by electric discharge machining. The proper selection of texture shapes, sizes, spacing's, and orientation is important to enhance the performance of lubricated contacts [23].

LST produces a very large number of micro-dimples on the surface and each of these micro dimples can serve either as a micro-hydrodynamic bearing in cases of full or mixed lubrication, a micro-reservoir for lubricant in cases of starved lubrication conditions, or a micro-trap for wear debris in either lubricated or dry sliding [24]. Study shows that surface texturing can reduce friction only if the dimple diameters are smaller than the contact width [12,25], while others show that friction increases under these conditions [26].

In an experiment pin on disc machine was used for measuring friction coefficients to see effect of LST by microdimpling on lubrication regime transitions during unidirectional sliding. LST expanded the range of the hydrodynamic lubrication regime for both high- and low viscosity oil lubricants in terms of load and sliding speed. After laser texturing, removal of the bulges at the edge of dimples by lapping is essential to optimize the beneficial effect of LST on lubrication regime transitions. Also, LST reduced the friction coefficient under similar operating conditions, when compared with untextured surfaces. It has been observed that a lower area dimple density is more beneficial for lubrication regime transitions. Hence, LST can be used to reduce friction in lubricated contacts that are operating under a boundary lubrication regime [27].

1.4. Methods of texturization

The simplest way to texture a surface for low friction is to make it rougher and then remove the protruding edges. Similarly, other techniques are laser and electron beam texturing. Now a days honing of cylinder surface and piston rings is done in combustion engines by cross hatching using some hard abrasives for better tribological properties. The texturing methods are abrasive jet machining (AJM), laser beam machining (LBM), lithography, deep x-ray lithography (DXRL), also known as (LIGA) and anisotropic etching. However, the most widely used technologies are laser surface texturing (LST) and reactive ion-beam etching (RIE). These methods are used to create micro dimples of different shapes, dimensions, depth, and distance between dimples on variety of material surfaces. LST is the most cost effective method, but a disadvantage of LST is the creation of bulges around dimples during the laser impulse impact and thermal cracks formation, especially on ceramics materials. Nevertheless, as numerous researches noted, the bulges could be easily removed by light polishing or at running-in period. RIE, AJM, LBM, lithography, LIGA technologies permit to produce dimples without material damages during texturing but these methods are more expensive [28].

1.5. Thesis structure

This thesis will cover the study that was done in the last year by Dmitrii Sergachev. He studied a lubricated contact of texturized flat surfaces against spherical ball using reciprocating tests with 2.5 mm stroke, ball of 10 mm in diameter and loads from 20 to 50N. The results obtained were not conclusive about the improvement that can be obtained by texturing.

1.5.1. Previous experimental approach

The coefficient of friction obtained by previous approach was very high for lubricated contacts. The values were from 0.15 to 0.2 for plain steel and 0.1 to 0.15 for coatings. Coatings delaminated at edges of textures while performing ball on disc test. It was caused by low contact areas in regards to groove width which caused lateral forces during ball deformation. It was reciprocating test, so speed increases from zero to maximum value.

Delamination's induced fluctuations in friction coefficient curves. Patterns with large dimple size should be tested against large flat surfaces to obtain sufficient results. Use of ball as a counter surface applies severe limitations on pattern dimensions, which increases texturing costs and not necessarily show better results in case of parallel surfaces. Textured surface area should be minimized along with the groove width to decrease abrasive wear and adhesion. Influence of counter surface velocity, load, sliding direction and lubricant viscosity on the optimal distance between grooves should be studied.

1.5.2. New experimental approach

The main objective of this research was to study effect of texturing to improve wear resistance and reduce friction in boundary lubrication regime in some tribological applications. The aim was to use same materials and texturing as Dmitrii Sergachev used in his study but changing experimental approach so that to get proper results to draw Stribeck curves. Following approaches were used in these experiments.

1.5.3. Contact geometry

Block on ring configuration was used instead of pin or ball on disc. It has following advantages. Contact area is large enough to study tribological effects on larger scales. In this way, normal load may be assumed as constant parameter to study effect of other parameters such as speed and viscosity. Furthermore, this contact geometry allows to study effect of texturing on larger contact area, which is expected to enhance the effect of the channel type available textures.

1.5.4. Unidirectional test

Test was unidirectional instead of reciprocating so as to get constant speed in whole test.

1.5.5. Stribeck curves

Samples with different pattern area density were used. Tests were performed with three lubricants with different viscosities. The Stribeck curve was obtained in one set of tests with constant normal load of 40 N by changing the rotational speed of disc in several steps. Different tests performed with un-textured and textured specimens under lubricated condition using three lubricants with different viscosities. The value of speed decides thickness of film and lubrication regime. So, it is easy at the end to get different data points for drawing a Stribeck curve.

2. Industrial problems and scope of texturization

2.1. Reciprocating automotive components

Energy losses resulting from friction between contact surfaces in an internal combustion engine have been studied intensively by a considerable number of tribologists. Still, the automotive industry needs further improvements to reduce friction-related energy losses in engines and drive systems. This problem can be solved by applying porous surfaces such as surface texturing. This work mainly focuses on tribological problems in sliding parts of automobiles combustion engines such as pistons with cylinders and polymer injection molding company.

Surface texturing in reciprocating automotive components also displayed a positive effect. In the Reynolds equation and the equation of motion are served simultaneously for as simplified “piston/cylinder” system with surface texturing. The solution provides behavior of both the clearance and the friction force between the “piston ring” and “cylinder liner” surfaces. It is shown that optimum surface texturing may substantially reduce the friction losses in reciprocating automotive components [29]. The experimental study evaluates the effect of partial laser surface texturing (LST) on friction reduction in piston rings. It was found that the partial LST piston rings exhibited about 25% lower friction [30-33].

Fuel consumption is an extremely important parameter for the automotive industry today. In engines the piston system is the largest source of frictional losses, accounting for about 30% of the total frictional losses, thus it is important to optimize. The lost caused by friction and wear is huge. There is about 30% power of automobile engine lost because of friction, 19% of the power loss is come from the piston ring-cylinder liner pair. This important pair of engine often damaged because of wear. Operational characteristics combined with the rings artificial texturing, influences the engine reliability and efficiency. Sliding components in automobiles combustion engine parts such as piston ring with cylinder and other machine parts operates at low sliding speeds and high load conditions. Therefore, coefficient of friction increases [34].

Proper lubrication and surface texture are key issues in reducing friction in a piston/cylinder system and, hence, have received great deal of attention in the relevant literature. Surface texturing as a means for enhancing tribological properties of mechanical components is well known for many years. Perhaps the most familiar and earliest commercial application of surface texturing in engines is that of cylinder liner honing. Surface texturing in general and laser surface

texturing (LST) in particular has emerged in recent years as a potential new technology to reduce friction in mechanical components [35].

2.2. Automobile engine mechanical components

2.2.1. Piston-cylinder system

2.2.2. Piston rings

Experimental study is presented to evaluate the effect of partial laser surface texturing (LST) on friction reduction in piston rings. In a previous study, 30% friction reduction was obtained with full LST where the full width of the piston ring is textured with a very large number of micro dimples that act individually as micro hydrodynamic bearings. In partial LST, only a portion of the piston-ring width is textured with high dimple density producing a “collective” effect of the dimples that provides an equivalent converging clearance even with nominally parallel mating surfaces [13]. I.Etsion and Y.Kligerman [2,13] found that a friction reduction of 30% and even more is feasible with textured surfaces. Figure 2.1 below shows partially and fully textured segments of piston rings.

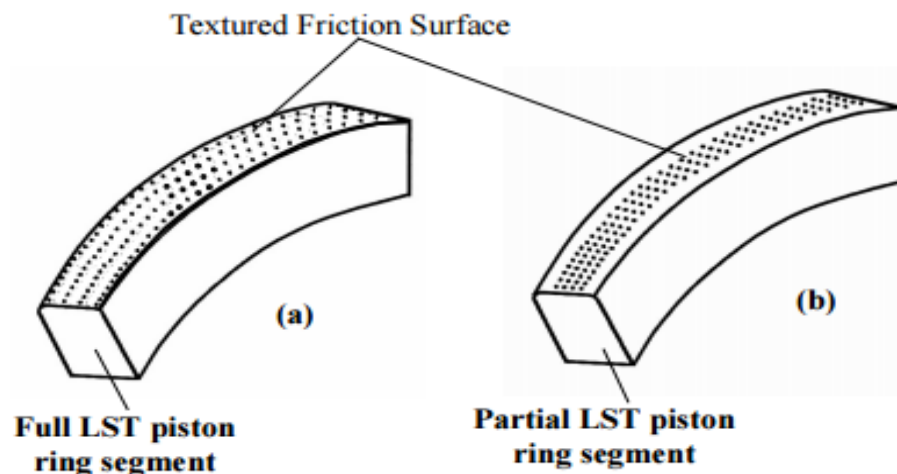


Figure 2.1. Segments of piston rings: (a) fully textured; (b) partially textured [13].

LST has a substantial effect on friction reduction compared to the non-textured reference rings. Piston rings were tested with partial surface texturing. Tests were performed on a reciprocating test rig with actual piston rings and cylinder liner segments. After this, comparison was made between the performance of a reference non-textured conventional barrel shape rings and optimum partial LST cylindrical shape rings. A model was developed to judge the potential of LST in Soft Elasto Hydrodynamic Lubrication. Significant friction reduction of about 20% can be achieved with optimum LST slider in comparison with a non-textured slider [36].

2.2.3. Seals, pumps and valves

Laser can be used to generate micro pores on T8 steel surface and the structure and morphology features of surface micro pores were observed. Tribological experiments were conducted with a ring-on-disc tester under various loads and speeds. It is shown that the maximum PV value of face seal can be increased by hydrodynamic effect of micro pores. Frictional properties of laser-micro pored surface were assessed through ring-on-disc tests, simulating a face seal contact interface with different loads and speeds. The findings are concluded as follows: All the surfaces had similar trends with the friction coefficients decreased at the initial stage and increased gradually with load and speed. Compared with the polished surface, the laser-micropored seal surface can improve the maximum PV value to 2.5 times. LST effectively increases load capacity and reduces friction in SEHL [18]. Textured surfaces have applications in fluid power systems such as seals, pumps and valves to significantly reduce friction and wear in these systems [16].

2.2.4. Cylinder liner

An optimal texturing design method on cylinder liner was proposed. It shows that on cylinder liner, texturing with variable parameters in different velocity ranges can produce higher load carrying capacity and film thickness than that with invariable parameters. The same results can be found at the top and bottom dead center, indicating that it is a good method to improve the hydrodynamic lubrication effect than others [37].

2.2.5. Mechanical Seals

In an experiment qualitative results of simulations showed that hydrodynamic force was dependent on rotational speed and the clearance height. Where pores were larger in depth and diameter on surface, the pressure was higher and so the hydrodynamic force. The smaller the radial distance between pores, the larger the hydrodynamic force was observed while no such effect was observed in circumferential direction. Figure 2.2 shows pores at SiC ring surface. The greatest effect of surface texturing was reported in the low-pressure zone [38].

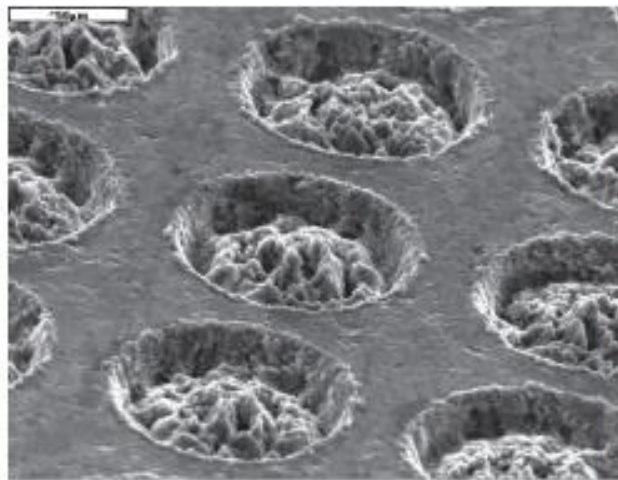


Figure 2.2. A view of pores on the SiC ring (magnification x25) [38].

2.2.6. Journal and thrust bearings

It was substantiated that improvement in tribological characteristics of journal and thrust bearing by surface texturing due to film thickness increasing. It was noted that the coefficient of friction can be reduced if a texture of suitable geometry is introduced. In addition, the literature revealed that in the mixed lubrication regime, the so-called secondary lubrication effect in dimpled area is the main mechanism responsible for performance improvement [39-43].

3. State of art

3.1. Basic theory of texturization

Figure 3.1 shows the creation of additional hydrodynamic force due to different hydrodynamic pressure distribution over diverging and converging parts of the dimple. The pressure decreases as the flow approaches the bottom center of the dimple. On the symmetrical side, the pressure increases. Figure 3.1 shows hydrodynamic effect of single idealized dimple.

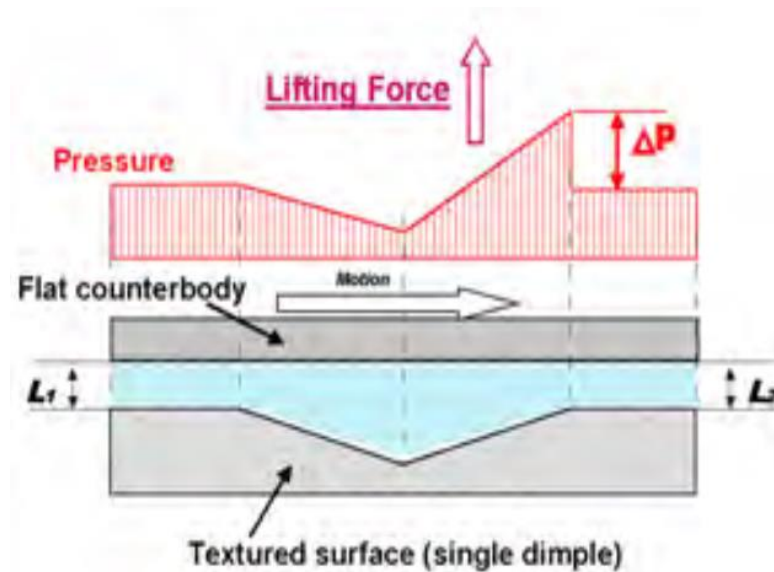


Figure 3.1. The hydrodynamic effect of the single idealized dimple [28].

Another effect acts on the condition of mixed lubrication between intimate contacting surfaces. The liquid trapped in the low region of the texture can be considered as a secondary source of lubricant, which is drawn by the relative movement to permeate into surrounding areas to reduce the friction and retard the galling. It is called the secondary lubrication effect [28].

Figure 3.2 below shows the simulation cell highlighting the texture geometry and the boundary conditions:

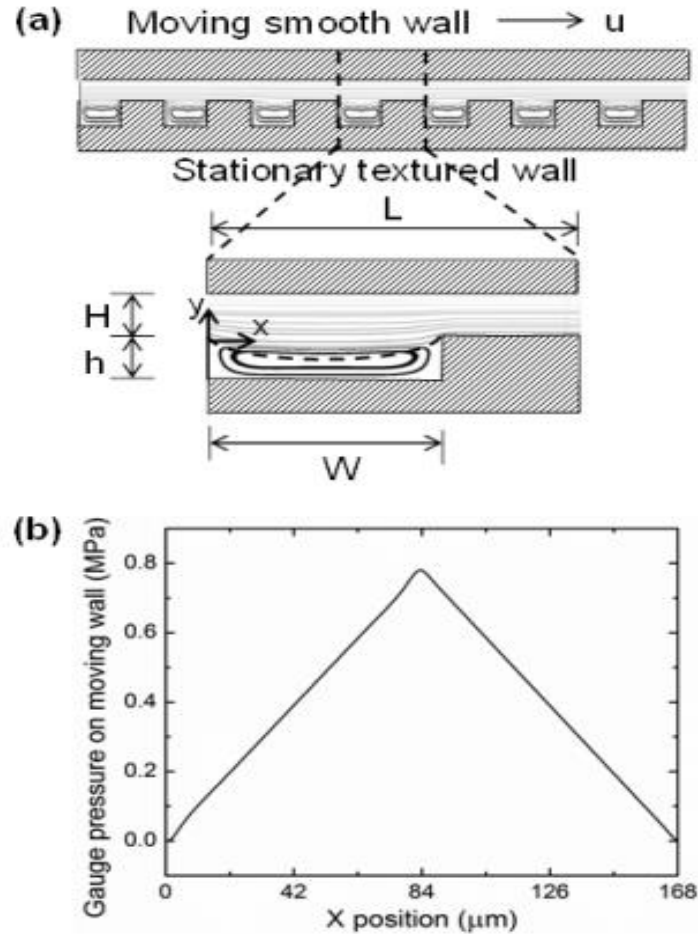


Figure 3.2. (a) Schematic of a computational cell with a moving smooth wall against a stationary textured wall with inlet textures, showing key geometry. (b) Prediction for pressure on top wall [16].

3.2. Use of dimples for textured surfaces

It is found that the tribological characteristics depended greatly on the size and density of the micro-dimples, whilst the dimple shape did not significantly affect the friction coefficient regardless of rounded or angular profiles. The results showed a large increase of the tool life when texturing of the substrate was made [44-45]. The direction of study to use dimples of textured surfaces as the reservoir for solid lubricant for providing a better working ability at dry friction is intensively developing. It is possible to achieve a significant reduction in friction coefficient and an increase in the wear life by choosing the optimal geometrical parameters of the textured surface with the subsequent treatment. The new mathematical models describing

tribological behavior of the textured surfaces are regularly appearing that can establish relation between structure and tribological parameters.

Studies suggest that texturing could be detrimental to tribological performance in non-conformal contact configuration. It was observed that relatively deep micro-dents in the lubricated contact results in fluid film thickness reduction and can cause lubricant film breakdown. For shallower dent, this effect is reduced, or even reversed for very shallow dents. As the conclusion, results suggest that surface texturing using microdents of an appropriate depth could help to increase lubrication films capabilities [46].

3.3. Spatial texture density

There is a certain spatial texture density at which the coefficient of friction is minimal. If a minimum coefficient of friction exists, then the most significant surface texturing parameter(s) which control the coefficient of friction need to be identified. When texturing size (D) is divided by distance between centers of two consecutive rectangular depressions (L), a minimum coefficient of friction is found at D/L equals to 0.4. D/L is called spatial texture density. Figure 3.3 shows dimensions of textured surface (spatial texture density) for 2D textured model.

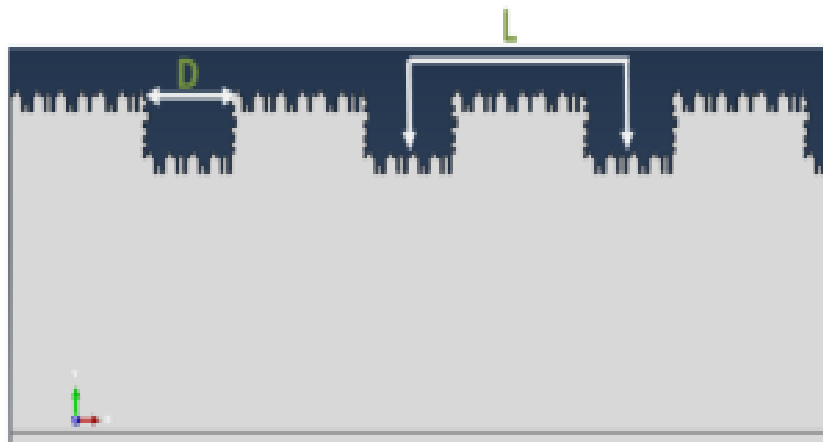


Figure 3.3.The Spatial Texture Density (D/L) for 2D Textured Model [46].

This quantity combines the effect of size and the density of the texture, thus it is very informative. The minimum coefficient of friction exists, and falls in a range of between 0.25 and 0.5 of the spatial texture density. The two friction components, mechanical deformation and

adhesion are inverse to each other when they are plotted vs. spatial texture density. As the spatial texture density increases, the adhesion decreases but the mechanical deformation increases. The behavior can be justified due to the change in real contact area which can be measured by the square of the complement of the spatial texture density (D/L). When the real area of contact decreases, the adhesion forces decrease. On the other hand, the mechanical deformation increases due to high stress concentration which result in the flow of material at the interface. The adhesion force decreases with increase of spatial surface texturing due to the reduction of the real area of contact. Figure 3.4 shows curve between spatial texture density and COF [46].

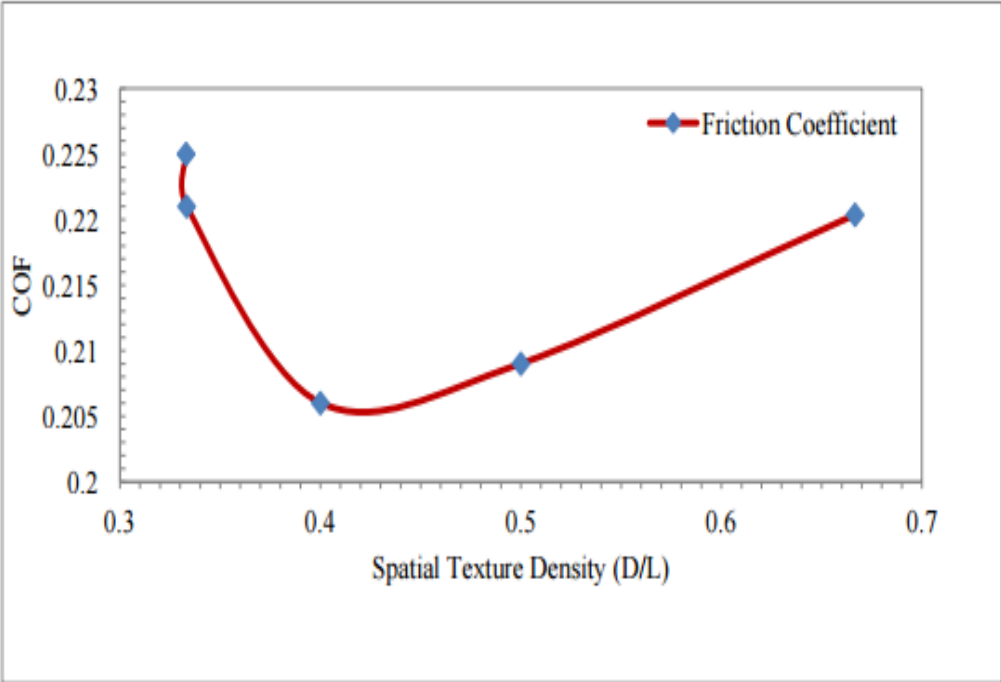


Figure 3.4.The Coefficient of Friction vs. the Spatial Texture Density (D /L) [46].

Hard coating is more beneficial in dry sliding conditions while surface texturing works better with lubricated sliding. It therefore seems reasonable to combine these two to obtain low friction and wear during sliding, the hydrodynamic force was greatly dependent on the rotational speed.

3.4. Effect of texturing on Stribeck curves

Load carrying capacity increases by incorporating texturing on the surface and Stribeck curves shifts towards left. The aim of this project was to design texturing on the surface and using various viscosity lubricants to lower the coefficient of friction and wear. Hence the purpose was to shift Stribeck curve to lower frictional values. Proper selection of pattern type and its dimensions can reduce coefficient of friction and wear rate. Combined effects of coating and texturing can give optimum properties for tribological surfaces.

Research work in the area of surface texturing, the way to modify contact surface through formation of suitable micro-dimples or micro-channels shows that improvement in friction and wear properties of contact surfaces can be expected. Different types of lubrication regimes exist depending on the operating conditions. The lubrication regimes are usually divided into three groups: boundary lubrication, mixed lubrication and hydrodynamic lubrication.

- **Boundary lubrication** Surfaces are in contact, the load is carried by the surface asperities.
- **Mixed lubrication** The load is carried by both the lubricant film and the asperities in contact.
- **Hydrodynamic lubrication** The surfaces are not in contact and a full film of lubricant, usually thicker than 1 μm , is carrying the load.
- **Elastohydrodynamic lubrication** It is a portion of hydrodynamic lubrication where some elastic surface deformation is possible.

In general, smoother surfaces are better for fluid film lubrication. Indeed, the effects of the film thickness and surface roughness on lubrication are combined in the so called ratio parameter defined as the ratio of the film thickness to the composite surface roughness. Eq. 1 shows specific film thickness is ratio between mean film thickness and composite surface roughness.

$$\text{Specific film thickness} = \lambda = \frac{\text{Mean film thickness}}{\text{Composite surface roughness}} \quad (1)$$

As long as the λ ratio is greater than unity, the film thickness exceeds the mean surface roughness and severe wear is minimized. When λ is less than one, the film thickness is smaller than the asperity height and the most severe wear regime exists (boundary lubrication). When λ becomes greater than four, even the highest asperities will no longer contact and ideal full film or hydrodynamic lubrication exists. In between these two extremes, λ is greater than one and less than four, is the mixed lubrication regime.

Coefficient of friction and film thickness are plotted against a parameter known as ‘Stribeck parameter’ which is equal to $\eta U/p$, where η is viscosity of oil, U is relative sliding speed and P is load per unit surface area of contact. The relationship between coefficient and film thickness in various regimes of lubrication can be qualitatively and quantitatively seen in [Figure 3.5](#) and [Table 3.1](#) below:

Table 3.2 Operating film thickness, Coefficient of friction and wear for various lubrication modes [47].

Lubrication mode	Film thickness μm	Friction coefficient
Hydrodynamic	1-10	$10^{-2} - 10^{-3}$
Elastohydrodynamic	0.1-1	$10^{-2} - 10^{-3}$
Externally pressurized	5-50	$10^{-3} - 10^{-6}$
Lubrication type		
Thick film	0.001	None
Boundary and mixed	0.05-0.15	Mild
Unlubricated or dry	0.5-2	Severe

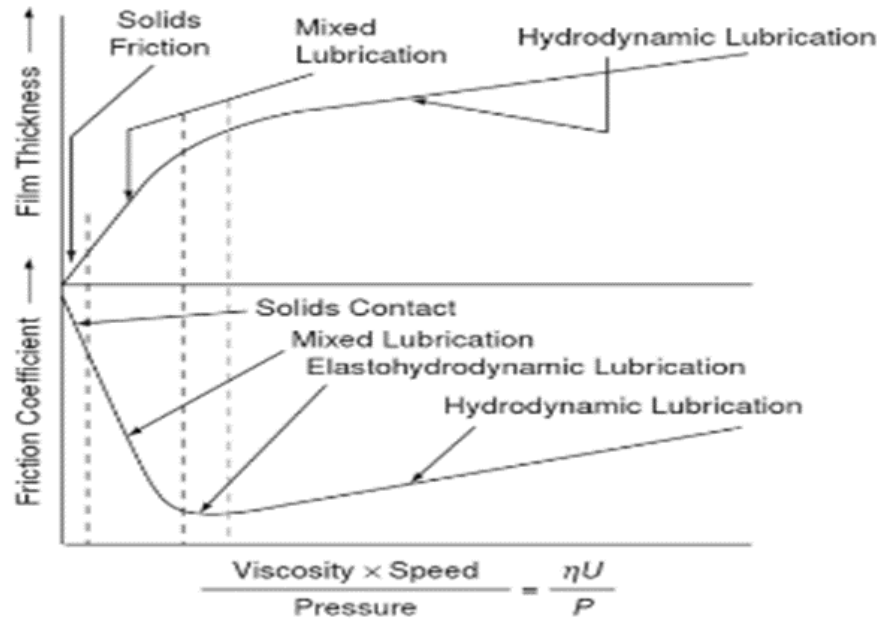


Figure 3.5.Stribeck curves showing modes of lubrication [47].

The test results showed that laser texturing expanded the contact parameters in terms of load and speed for hydrodynamic lubrication, as indicated by friction transitions on the Stribeck curve. The beneficial effects of laser surface texturing are more pronounced at higher speeds and loads, and with higher viscosity oil [27,48]. Figure 3.6 shows Stribeck curves of ground, polished and textured (dimple) surfaces.

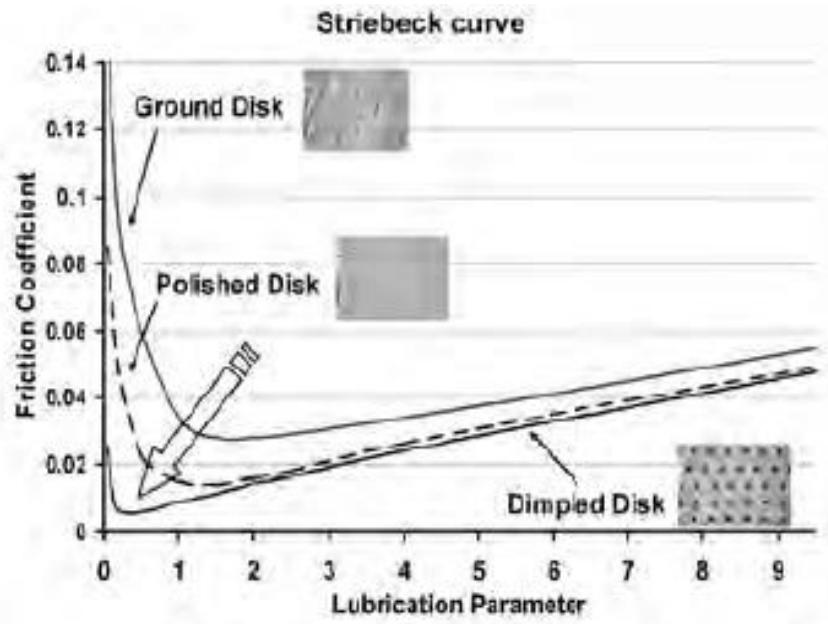


Figure 3.6. The Stribeck curves of the ground, polished and dimpled (textured) [27].

The [Table 3.2](#) below lists the textures tested, the operating conditions and the manufacturing methodology used to produce these microscale textures. [Table 3.3](#) shows the key literature in numerical study of micro textured surfaces. Key parameters like texture geometry, operating conditions and the numerical model are listed. Conclusions drawn in terms of the optimum texture parameters for these conditions are also listed in the table. Micro textured surfaces can find application in seals, pumps and valves to significantly reduce friction and wear in these systems.

Table 3.2. Summary of literature in the experimental domain and the key parameters studied [16].

Author	Regime	Texture width (μm)	Texture depth (μm)	Lubricant	Viscosity @20C (Pa.s)	Pressure MPa	Velocity m/s	Texture material	Texture method
Geiger (1998)	HD, EHL	25-150	5-20	Mineral oil	1.5		1-2	Ceramic	LST
Dumitru (2000)	HD, BL	5-10	5-8	Mineral oil	0.096 @40C		0.01	440 Stainless	LST
Ryk (2002)	HD	100	8-11, 19, 20	SAE 40	0.113 @40 C	0.1-0.5		Chrome coated steel	LST
Wang (2003)	HD	50-650	2-16.6	Water	0.001	1.5-15	0.31-0.94	SiC	RIE
Pettersson (2003)	BL	5, 20, 50	5	Poly-alpha olefin		680	0.0125	TiN, DLC on Si	PL and KOH etch
Pettersson (2004)	BL	5, 20, 50	5	Poly-alpha olefin		680	0.15-0.75	52100 steel	PL and KOH etch
Kovalchenko (2004)	BL-HD	58-140	4-6.5	10W30 15W50	0.047, 0.11 @40 C	0.16-1.6	0.15 – 0.75	Cast iron	LST
Nakano (2007)	HD	60, 500	6-10, 45-50	VG 68	0.059	1.6	0.083 - 1.0	steel	Shot blasting
Pettersson (2007)	BL	5-20		Mineral oil	0.02	100	0.006	steel	PL and chemical etch
Costa (2007)	HD	40-130	1.8-8	Mineral oil	1.5	9.4-24.1	0.0121	steel	PL and DRIE
Nakano (2009)	HD	30-40	10-12	VG 32, 68, 320	0.026-0.27	0.014-0.140	0.001-0.005	NiFe on Si	LST
Qiu (2011)	HD	250-2000	46-60	SAE 30 engine oil			0.05-4.2	17-4PH stainless	LST
Yamakiri (2011)	BL	11-35	8-24	water	0.001	0.1-0.8	0.042-0.25	Si ₃ N ₄	LST
Surya (2011)	BL	40-60	4-10	PAG, POE	0.06	5.71	0.96-3.84	Cast iron	LST
Mitchell (2012)	HD	10 - 100	5-60	N35 mineral oil	0.06		0.01	316L stainless	μ -casting

Table 3.3. Summary of literature in the numerical domain and the key parameters studied [16].

Author	Regime	Model	Texture geometry	Viscosity (Pa.s)	Pressure (MPa)	Velocity (m/s)	Application
Etsion (1996)	HD	Reynolds	Hemispherical dimples	0.001	0.5-3	9.5	Mechanical seals
Ai (1996)	EHL	Reynolds	Transverse, longitudinal, oblique roughness	0.04	230 – 380		High pressure seals
Ronen (2001)	HD	Reynolds	Spherical dimples				Reciprocating automotive
Arghir (2003)	HD	NS	Rectangular, Sinusoidal, Triangular C/S	Re: 0.1- 100			Various applications
Siripuram (2004)	HD	Reynolds	Circle, Square, Diamond, Hex, Triangle	0.042	0.1	2.66	Mechanical seal
Sahlin (2005)	HD	NS	Cylindrical, splined C/S	Re: 40 - 160			Various applications
Brajdic (2005)	HD	NS	Square pockets	0.009	0.5-50	1	Pad bearing
Kligerman (2005)	HD	Reynolds	Partial textures with spherical dimples	0.083	0.4	4.8	Piston rings
Dobrica (2009)	HD	Reynolds and NS	Square pockets	Re: 0.125 – 256			Various applications
Dobrica (2010)	HD	Reynolds	Trapezoidal textures – Partial and full	0.03	FT = 15 μ m	5	Pad bearing
Han (2010)	HD	NS	Spherical dimple	Re: 10 – 160			Various applications
Qiu (2011)	HD	Reynolds	Spherical dimple	0.0002 – 1	FT = 2 – 24 μ m	0.63 – 3.77	Thrust bearing, mechanical seal

3.4.1. Effects of texture size, shape, area fraction, and orientation

Hsu [49] showed for the first time the influence of geometric shape (circle, ellipse and triangle) and orientation effects on friction reduction under high speed (speed range: 0.023-0.23 m/s), low load conditions (pressure: 0.03-1.1 MPa). In order to study the orientation effects with respect to sliding direction, Hsu [49] considered the following features, presented in Table 3.4.

Table 3.4. Features of surface texture [49]



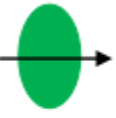


Pattern	Circle	Ellipse		Triangle	
Sliding direction					
Nomenclature	Circle	Ellipse A	Ellipse W	TV	TA

Table 3.4 provided an overview of the effects of features of various shapes and orientations. The results present effect of paraffin oil-lubricated sliding friction experiments at two speeds: 0.023 and 0.23 m/s, and 1-40 N loads, using circles, triangles, and oval shaped features produced by lithography and etching. Depending on the sliding speed and orientation of the features relative to the sliding direction, the effects on kinetic friction coefficient (COF) were different:

- Circles (at low speed): COF increased with increasing load and produced noisy friction traces
- Circles (at high speed): COF decreased rapidly with load from 1-5 N, and then remained relatively low and stable.
- Ellipses (at sliding parallel to the long axis at low speed): COF increased with increasing load and produced moderately noisy friction traces
- Ellipses (at sliding parallel to the long axis at high speed): COF decreased with increasing load from 1-5 N and produced stable friction traces
- Ellipses (at sliding perpendicular to the long axis at low speed): COF increased gradually with increasing load and produced moderately noisy friction traces
- Ellipses (at sliding perpendicular to the long axis at high speed): COF decreased with increasing load and produced stable friction traces

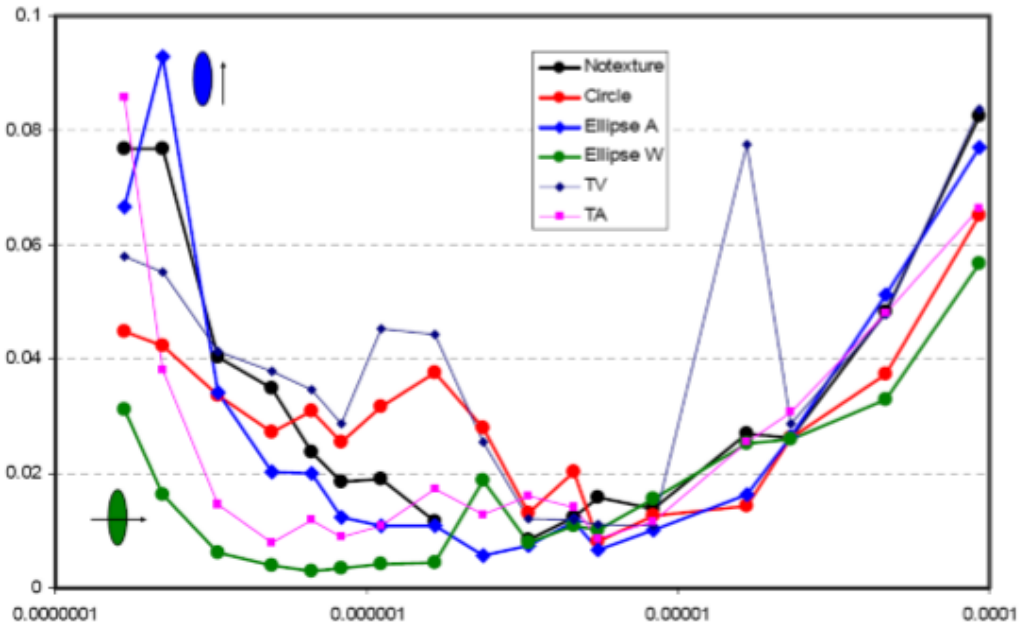


Figure 3.7. Effect of shape and orientation of texture on friction [50].

As shown in Figure 3.7, Hsu [49] concluded that dimple shape could have some effect, and that, in particular, shapes with an orientation more perpendicular to the sliding direction, as seen for ellipse A could delay the onset of asperity contact. Results also indicated that round dimples (circle) had almost no effect. However, in disagreement with Hsu, Stephens and Siripuram [50] considered circular, square, diamond, hexagonal and triangular cross-sections, and concluded that friction reduction was generally independent of shape.

Pettersson and Jacobson [12] conducted an experimental study where the influence of the pattern shape (square depressions or parallel grooves), size and orientation of textures (along or perpendicular to sliding direction) was investigated on diamond-like carbon (DLC) coated surfaces under starved and abundantly lubricated conditions. Figure 3.8 shows a summary of the performance of the textured surfaces where the circles represent the elastic contact area according to Hertzian calculations with a load of 5 N (680 MPa). The depressions (grooves and squares) are of the three different widths: 5, 20 and 50 μm . The 20 and 50 μm textures are all 5 μm deep, while the 5 μm textures are 3.5 μm deep.

According to this study, the best results in terms of friction reduction were achieved in the starved boundary-lubrication mode. As evident from the Figure 3.8, successful textures exhibit either: a dense pattern of depressions within the active contact area, or a less dense texture but an

orientation that ensures that each part of the contact area frequently passes over a depression. Less successful friction and wear behavior was exhibited by textures with sparse depressions (or no depressions) and by textures that for local parts of the contact area allow long sliding distances without passing an oil reservoir [12].

Under boundary lubricated conditions with an ample oil supply, this study [12] showed that the friction was rather insensitive to the choice of texture. However, other investigators have found beneficial influences of the textures with an ample supply of oil, but at substantially lower pressures [51].



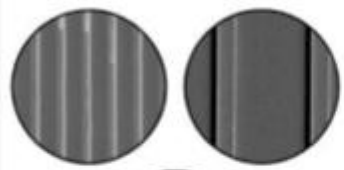





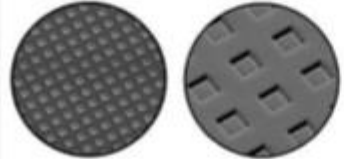

Surface texture (orientation)	Low friction and no measurable wear	High friction and severe wear
Sliding direction of the balls 		
Flat reference		
Grooves (perpendicular to sliding direction)		
Grooves (along sliding direction)		
Square depressions (along sliding direction)		
Square depressions (30° from sliding direction)		

Figure 3.8. Summary of the performance of the textured surfaces in starved boundary lubricated sliding [12].

Surface texture controls interfacial properties such as area of contact, contact pressure, stress concentration, interfacial temperatures and fractional resistance. Stribeck curves generally moves left and down due to effect of texturing. The shape of texture to sliding body also affects the coefficient of friction. The perpendicular texture gives constrained flow for metal during sliding which results in higher values of coefficient of friction but a random texture gives less constrained flow of material which results in lower values of coefficient of friction. The coefficient of friction also depends upon ability of surface to retain lubricant and thickness of fluid film generated during sliding [52].

3.4.2. Effect of sliding velocity and lubricant viscosity on film thickness

It was found that speed of sliding bodies and lubricant viscosity affected by the minimum film thickness at point of contact. Increasing speed of sliding bodies increased lubricant film thickness while increasing load decreased lubricant film thickness [53].

Friction among non-conformal contacts decreases by increasing the entraining velocity. This is because of rise in temperature at sliding contact by increasing the entraining velocity. The results of [55] showed that Stribeck curve is influenced by viscosity of lubricant and it can be seen in Figure 3.9 below:

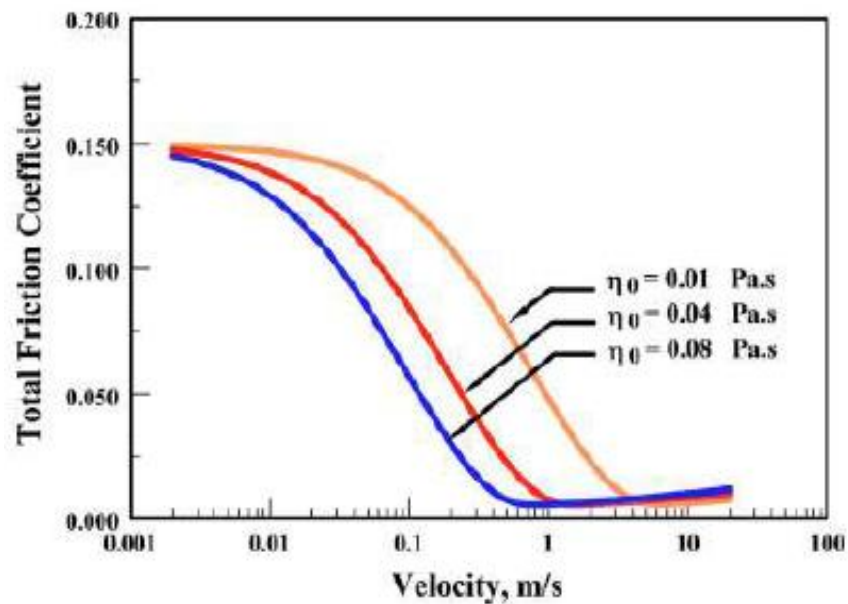


Figure 3.9. Effect of viscosity on Stribeck Curve [54].

It was also noticed that under the specific loads condition, grooves orientation perpendicular to sliding direction have successful texturing effect. The surface texturing can also effect regimes of lubrication. Hydrodynamic regime can be extended for a greater load and speed. It was found that lower coefficient of friction is attained by laser surface texturing when compared with a polished surfaces. The increase of load carrying capacity and friction reduction particularly at low speeds is confirmed by experimental work [55].

4. Materials and Methods

The minimum film thicknesses (h_0) have been calculated for the isothermal elastohydrodynamic lubrication conditions using the equation of Hamrock and Dowson [56,57] presented below Eq. (2). This equation applies to any contact, such as linear (flat on ring) and can be used for many material combinations up to maximum pressures of 3-4 GPa.

$$\frac{h_0}{R'} = 3.63 \left(\frac{U\eta_0}{E'R'} \right)^{0.68} (\alpha E')^{0.49} \left(\frac{W}{E'R'^2} \right)^{-0.073} (1 - e^{-0.68K}) \quad (2)$$

Where:

h_0 is the minimum film thickness [m];

U is the entraining surface velocity [m/s], i.e. $U = (U_A + U_B)/2$, where the subscripts 'A' and 'B' refer to the velocities of bodies 'A' and 'B' respectively;

η_0 is the viscosity at atmospheric pressure and temperature ' θ ' of the lubricant [Pas];

E' is the reduced Young's modulus [Pa];

R' is the reduced radius of curvature [m];

α is the pressure-viscosity coefficient [m^2/N];

W is the contact load [N];

k is the ellipticity parameter defined as: $k = a/b$, where 'a' is the semiaxis in the transverse direction and 'b' is the semiaxis in the direction of motion. For line contact $k = \infty$.

The lubricant fluid used in these calculations is assumed to be compressible and its viscosity-pressure behaviour is described by the Barus law Eq. (3). However, according with Sargent et al. [58] the application of this equation to pressures above 0.5 GPa can, lead to serious errors.

$$\eta_p = \eta_0 e^{\alpha p} \quad (3)$$

Where:

η_p is the lubricant viscosity at pressure 'p' and temperature ' θ ' [Pas];

In order to account for surface roughness in the calculation of the film thickness. Tallian [33], proposed a new parameter characterizing the ratio of the minimum film thickness to the composite surface roughness, and is defined as:

$$\lambda = \frac{h_0}{(\sigma_A^2 + \sigma_B^2)^{0.5}} \quad (4)$$

Where:

σ_A is the RMS surface roughness of body 'A' [m];

σ_B is the RMS surface roughness of body 'B' [m];

λ is the parameter characterizing the ratio of the minimum film thickness to the composite surface roughness.

4.1. Types of Pattern

4.1.1. Specimens

The steel specimens of quenched and tempered (710 HV) AISI M2 steel were prepared by machining and polishing to mirror smoothness ($R_a = 0.01 \mu\text{m}$). The chemical composition can be seen in Table 4.1. The size of each specimen was $\varnothing 20 \times 7.8$ mm. All the disc specimens were textured by wire EDM by positioning it parallel to the surface with three different patterns of micro-grooves, different in terms of patterned area density. Patterned area density was calculated by dividing the surface into equal triangles as shown in Figure 4.1. Intersection angle was 60 degrees and width of the grooves (t) were $150 \mu\text{m}$, respectively. Patterned area density was varied by changing the distance between grooves (d).

Table 4.1. Steel chemical composition (in weight %).

Chemical composition	C	Cr	Mn	Mo	Ni	V	Si	W
AISI M2	1.00	4.15	0.30	5.0	-	1.95	0.30	6.25
AISI 3415	0.17	0.75	0.55	-	3.25	-	<0.20	-

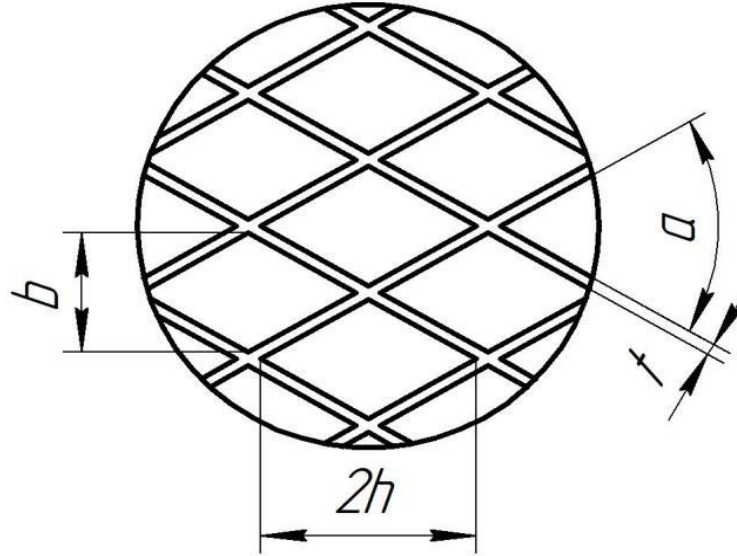


Figure 4.1. Pattern geometry and dimensions.

The ratio of surface area to the whole area was represented as ratio of the areas of similar triangles, which, by their properties, is equal to squared coefficient of similarity. Therefore, patterned area density was calculated as:

$$A_p = 1 - \left(\frac{b}{b + \frac{t}{\cos(\alpha/2)}} \right)^2 \quad (5)$$

Where A_p is the pattern area density, b the rhomb width, t the groove width and α the intersection angle. The distance between grooves can be expressed as $d = b \cos(\alpha/2) + t$.

The main feature characteristics of the three textured patterns were measured with white light 3D scanning microscope and average measured and calculated values, which fully characterize textured samples are presented in [Table 4.2](#). After EDM texturing, the disc specimens were polished again to remove uniform grinding marks and achieve similar surface roughness as the smooth specimen. [Figure 4.2](#) shows the three surface textured patterns with 21, 44 and 65 % area densities, corresponding to the designation of TLowD, TMediumD and THighD, respectively.

Table 4.2. Main features characteristics of the textured disc patterns.

Surface texture pattern	TLowD	TMediumD	THighD
Distance between grooves, d (μm)	1294	603	390
Groove width, t (μm)	142	149	159
Groove depth (μm)	16.3	15.8	17.8
Rhomb width, b (μm)	1331	524	267
Patterned area density, A_p (%)	21	44	65

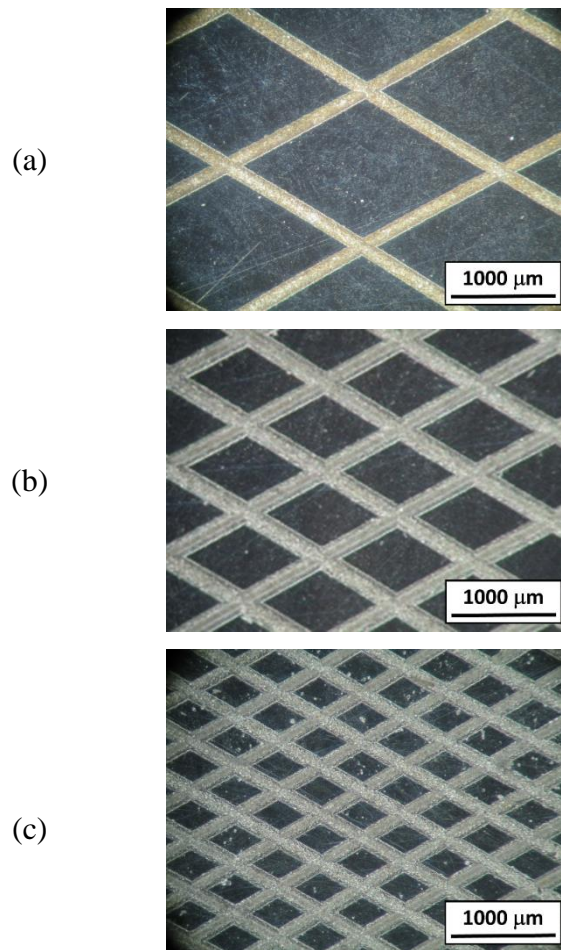


Fig. 4.2. Micrographs of surface textured patterns: (a) textured with low density-TLowD (b) textured with medium density-TMediumD and, (c) textured with high density-THighD.

4.2. Characterization of samples surface

An example of a 2D profile of a textured surface with low density – TLowD is presented in Figure 4.3. Figure 4.4 shows area for one cone, the groove depth is approximately 16 μm . It can also be seen that the groove edges exhibit a perfect round shape and depth.

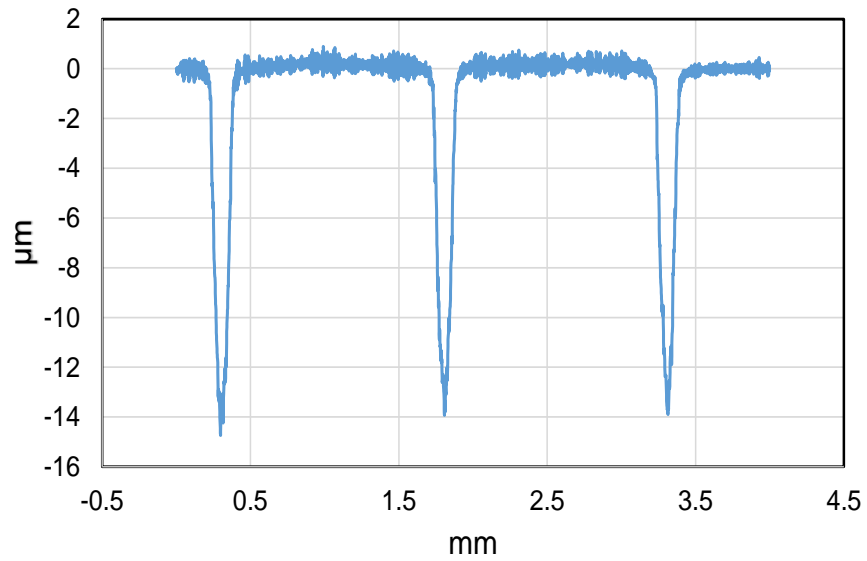


Figure 4.3. 2D profile of TLowD specimen illustrating the shape and dimensions of typical micro-grooves.

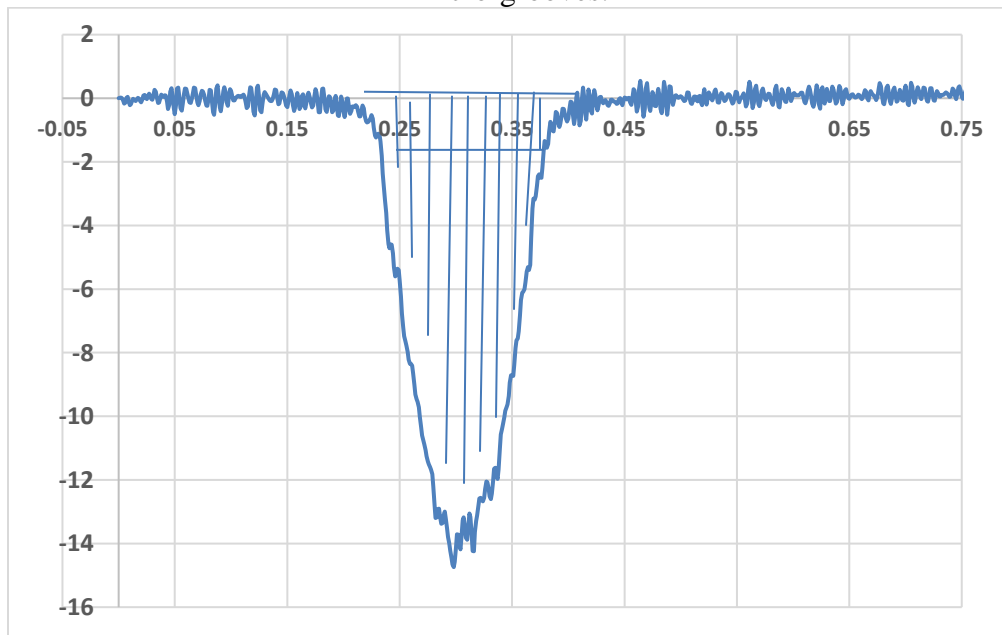


Figure 4.4. Roughness profile (single cone).

4.3. Calculation of cone area

To calculate area for one honed surface, the whole surface should be divided into trapezes. The area of all trapezes is calculated and then added. The formula for calculating area of one trapeze is as follows:

$$A_i = (Y(i-1) + Y_i) * \frac{(X_i - X(i-1))}{2} = 1.41 * 10^{-03} \text{ mm.} \quad (6)$$

Patterns were made with EDM technique. Textured samples were grinded afterwards with SiC paper grit 4000 to remove grinding marks.

4.4. Experimental procedure

Block on ring sliding test tribometer used in this testing is shown in [Figure 4.5](#).

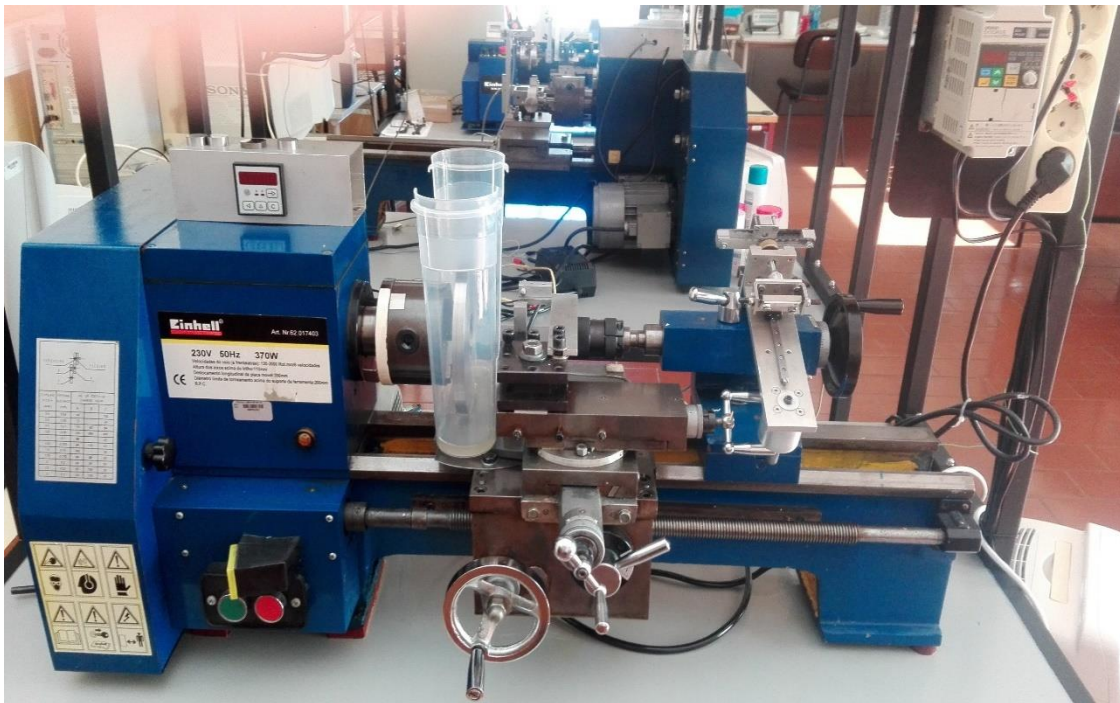


Figure 4.5. Block on ring sliding test tribometer used for testing.

Friction tests were carried out using a block-on-ring friction machine under unidirectional sliding. The Schematic diagram of the block-on-ring sliding test tribometer can be seen in [Figure 4.6](#). During test stationary block consisting of the four different test specimens three textured and one un-textured was pressed with a constant load of 40 N against a rotating ring. The rotating ring is 150 mm in diameter and 12 mm in thickness and is made of alloyed carbon steel (3415, AISI). Specimens were positioned 90° to the ring's axis of rotation. The chemical composition of the rotating ring is given in [Table 4.1](#). The initial surface roughness of rotating ring was $R_a = 0.04 \mu\text{m}$. During tests, normal load and friction force between the sliding surfaces of the block and ring were monitored, thus computing values of friction coefficient. The effect of sliding speed and the patterned area density on the friction behaviour were investigated. The friction tests were conducted on low density texture, medium density texture and high density texture discs at a normal load of 40 N for the six different linear sliding speeds mentioned below.

According to the Hertzian stress theory, this applied load corresponds to a nominal contact pressure of approximately 0.04 GPa. However, the real contact area decreased due to the grooves for a pattern area ratio between 21 and 65 %, leading to an increase real contact pressure. Results were then compared to un-textured case and presented in the form of coefficient of friction as a function of textured patterned density. Tests were carried out at angular speeds of 4, 13, 32, 64, 127 and 162 rpm, corresponding to linear sliding speeds of 0.03, 0.1, 0.25, 0.5, 1.0 and 1.27 m/s, respectively. The number of turns was set to 100, 250, 500, 1000, 1000 and 1000, respectively.

During testing, three different oils were used as lubricants: ISO VG 46 (PAO 8, $\nu_{40} = 46 \text{ mm}^2/\text{s}$), ISO VG 150, synthetic based products formulated with a combination of PAO ($\nu_{40} = 150 \text{ mm}^2/\text{s}$) and ISO VG 320, also formulated with a combination of synthetic based products and PAO ($\nu_{40} = 320 \text{ mm}^2/\text{s}$). The main oil properties can be seen in [Table 4.3](#). The lubricating conditions were set to fully flooded contact. Each test was started with ultrasonically cleaned and dried disc and block surfaces. The atmosphere surrounding the test was room air of $22 \pm 2^\circ\text{C}$ and relative humidity of $58 \pm 10\%$. Each friction test was carried out for the sliding distance of 47, 118, 236, 471, 471 and 469 m (corresponding to the running conditions defined above), during which the steady-state conditions were reached. Error bars were estimated from standard deviations of steady coefficient of friction values.

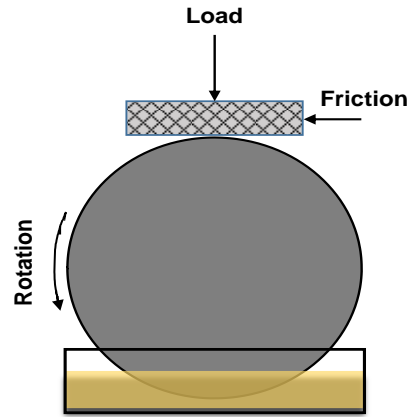


Fig. 4.6. Schematic diagram of the block-on-ring sliding test tribometer.

Table 4.3. Lubricant properties.

Oil	Kinematic viscosity (mm²/s) @ 40⁰C	Density (g/cm³) @ 15⁰C
ISO VG 46	46	0.830
ISO VG 150	150	0.872
ISO VG 320	320	0.903

5. Results and discussion

5.1. Effect of lubricant viscosity and pattern area density on COF

5.1.1. ISO VG 46 (PAO8)

Figure 5.1 shows the steady state values of coefficient of friction for un-textured and textured surfaces lubricated with PAO8 for the six different sliding speeds. It can be seen that for all the samples, the friction shows a clear evolution from a high coefficient of friction values at low sliding speeds to a lower friction values at higher sliding speeds. The curves showed that textured surfaces had no beneficial effect in reducing friction at low sliding speeds (from 0.03 up to 0.25 m/s). However, the textured surfaces start to show positive effect at higher sliding speeds (from 0.5 up to 1.27 m/s). It can be seen that for higher sliding speeds, the beneficial effect of the grooved surface texturing becomes larger as the texture density decreases. The curve for high density textured sample has the highest coefficient of frictions while the curve of medium density textured sample has coefficient of frictions in between low density and high density textured samples.

In a previous study [25,26], It was also found that the tribological behaviour depends on the depth of the micro-dimples as well as on the operating conditions with the beneficial effect becoming larger for higher sliding speeds. Moreover, the patterns with micro-dimples have closed textured surfaces and they are supposed to retain the lubricant and to generate hydrodynamic pressure easier than micro-grooves. It was also observed that patterns with micro-grooves with low and medium densities used in this study seem to play a positive role in preventing side leakage of the lubricating oil and decreasing the coefficient of friction in relation to the smooth surface. This could be explained due to the geometry of the grooves that have interconnected rhombic form instead of a linear and open geometry.

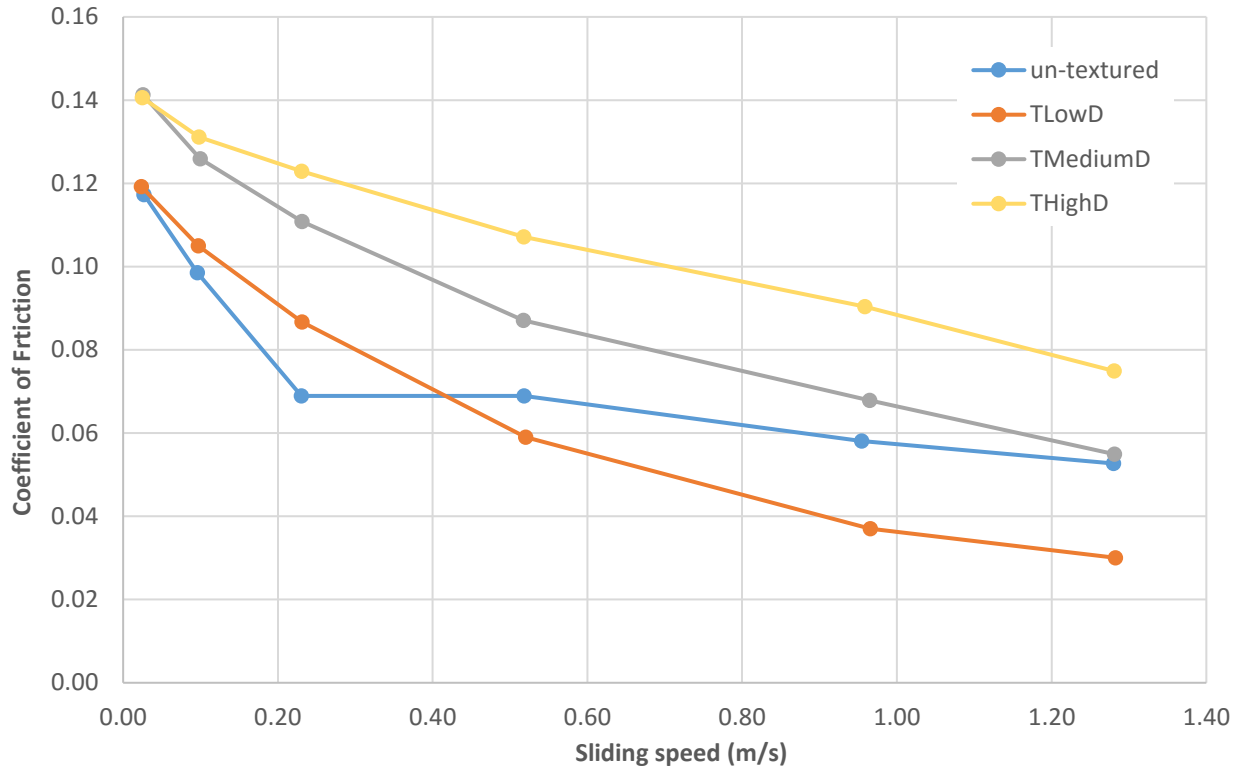


Figure 5.1. Variation in coefficient of friction with sliding speed for un-textured and textured surfaces lubricated with ISO VG 46: $\nu_{40} = 46 \text{ mm}^2/\text{s}$ and at 40 N applied load.

5.1.2. High viscosity oil – ISO VG 320

Figure 5.2 shows the variation of the steady-state coefficient of friction for un-textured and textured surfaces lubricated with ISO VG 320, for the six different sliding speeds (0.03, 0.1, 0.25, 0.5, 1.0 and 1.27 m/s).

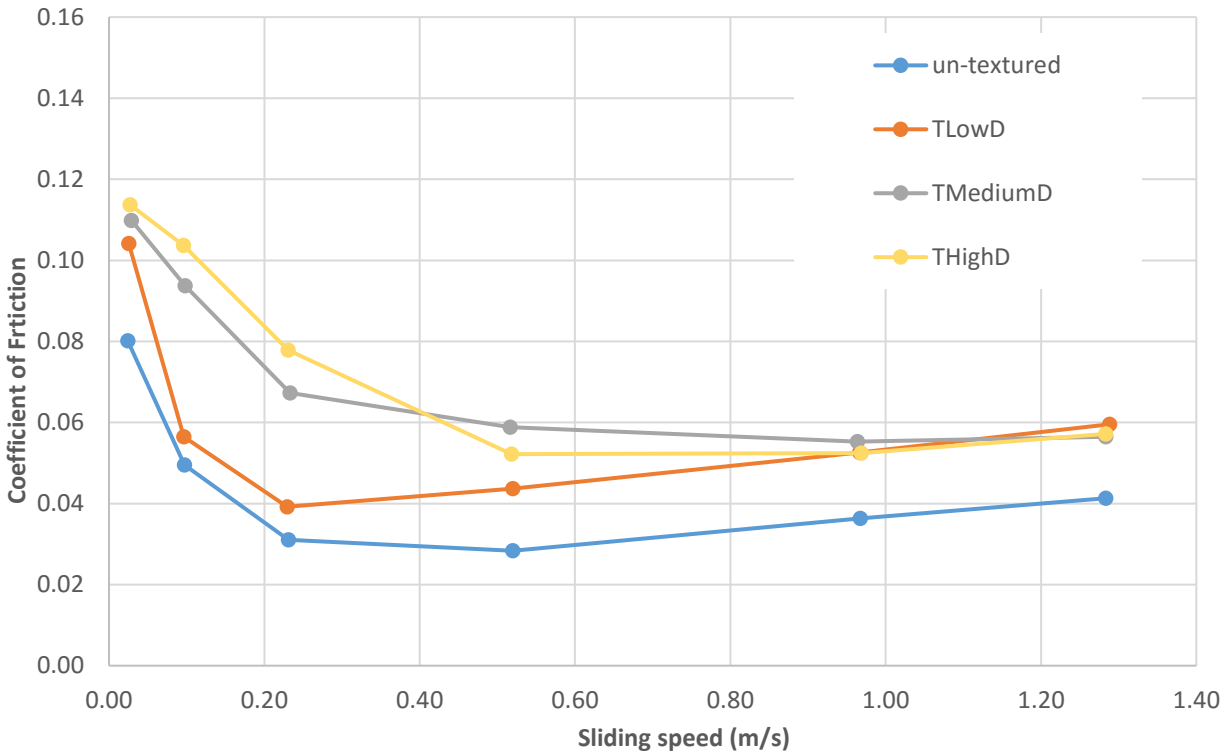


Figure 5.2. Variation in coefficient of friction with sliding speed for un-textured and textured surfaces lubricated with ISO VG 320: $\nu_{40} = 320 \text{ mm}^2/\text{s}$ ($F_N = 40 \text{ N}$).

5.1.3. Medium viscosity oil – ISO VG 150

Figure 5.3 shows the variation of the steady-state coefficient of friction for un-textured and textured surfaces lubricated with ISO VG 150, for the six different sliding speeds (0.03, 0.1, 0.25, 0.5, 1.0 and 1.27 m/s).

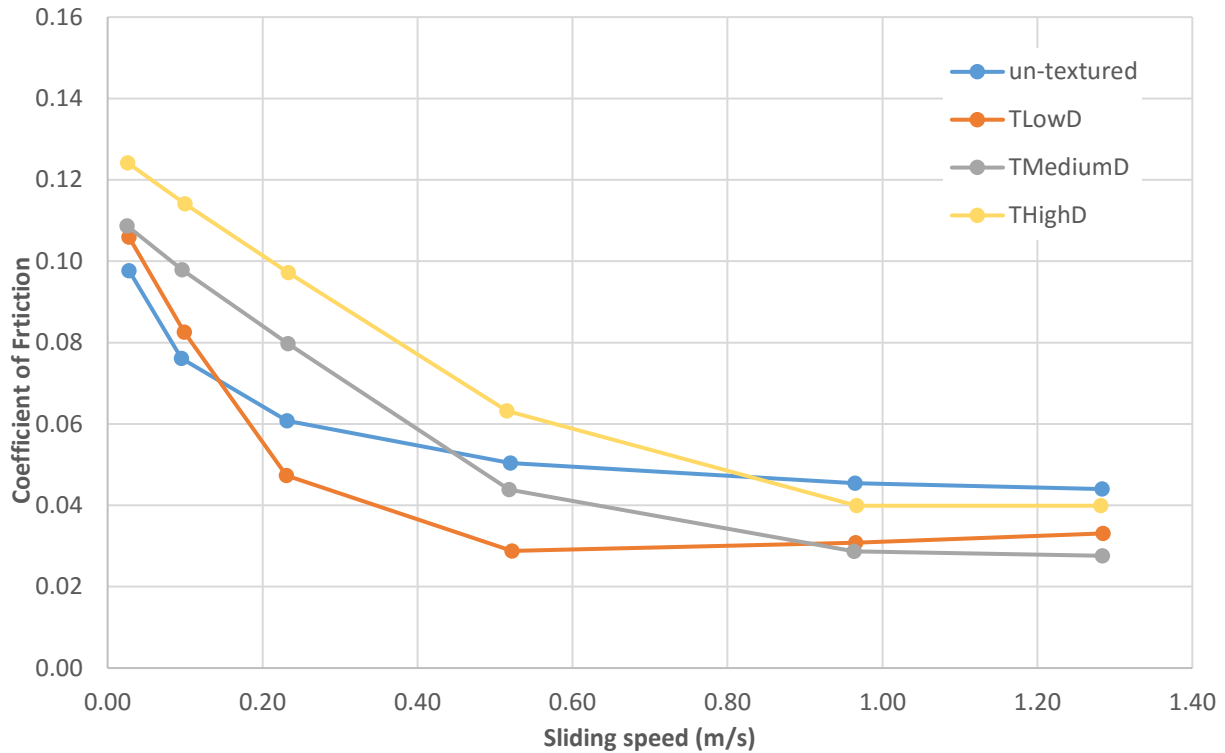


Figure 5.3. Variation in coefficient of friction with sliding speed for un-textured and textured surfaces lubricated with ISO VG 150: $\nu_{40} = 150 \text{ mm}^2/\text{s}$ ($F_N = 40 \text{ N}$).

5.2. Comparison between different lubricant viscosities

5.2.1. Comparison between low viscosity (ISO VG 46) and high viscosity (ISO VG 320) oil

Figure 5.4 shows the comparison of coefficient of friction values for un-textured and textured surfaces lubricated with ISO VG 46 and ISO VG 320 for the six different sliding speeds. It can be seen in Figure 5.4 that curves change drastically with increasing oil viscosity from 46 to 320 mm^2/s . Two main effects can be observed. First, transition from a boundary, mixed and hydrodynamic lubrication regime occurred at lower sliding speeds for higher viscosity (320 mm^2/s) oil. Second, the slope in the hydrodynamic lubrication regime increases with increasing viscosity and it can be seen for dashed lines shown in Figure 5.4.

It was observed for higher viscosity oil ISO VG 320 (curves shown by dashed lines in Figure 5.4) that at lower sliding speeds, specimens showed lower coefficient of friction than specimens lubricated with lower viscosity oil ISO VG 46 (shown by solid lines in Figure 5.4). It can be seen for both lubricants that coefficient of friction is increasing as the pattern area density increases from low density texture (TLowD) to medium density texture (TMediumD) and up to high density texture (THighD). The reason for this is, as pattern area density increases, the real contact area decreases due to presence of grooves and this lead to an increase of the real contact pressure and increasing coefficient of friction.

The smooth specimen is showing the lowest coefficient of friction of all specimens. As we moved towards higher sliding speeds the differences between the coefficient of friction for un-textured and textured discs become smaller due to the increase in lubricant viscosity, resulting in increasing lubricant film thickness as sliding speed increases.

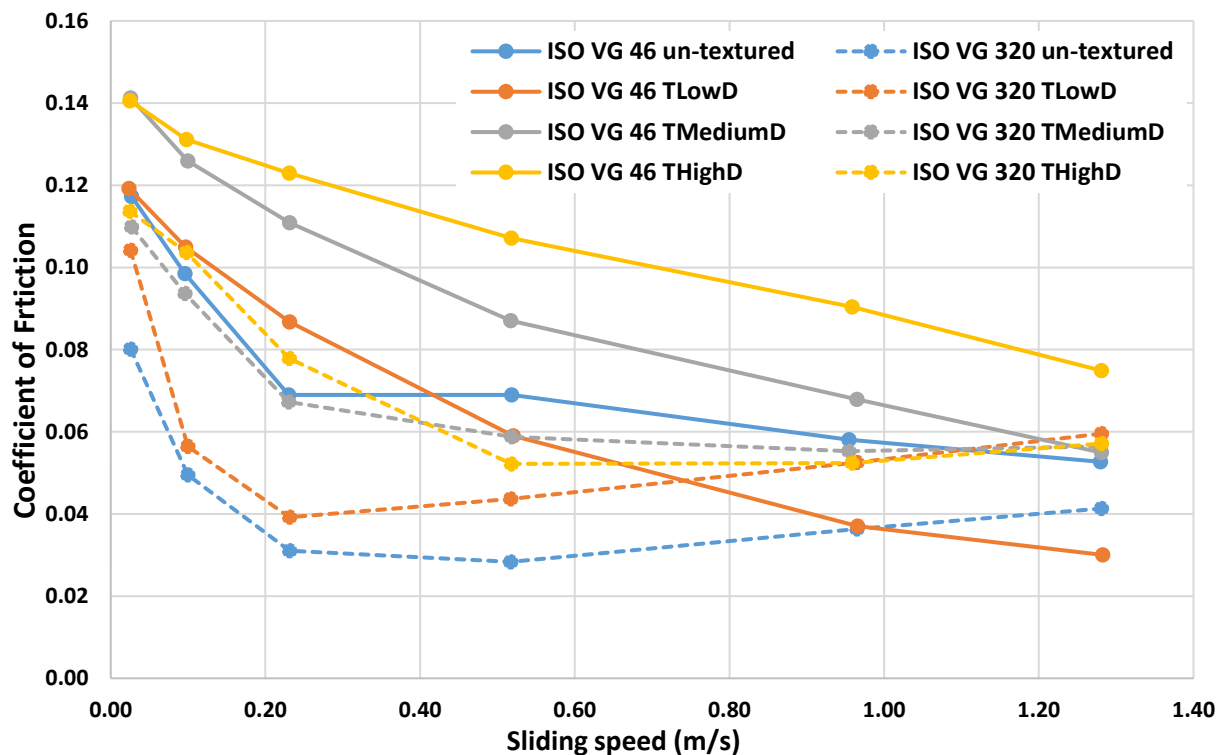


Figure 5.4. Variation in coefficient of friction with sliding speed for un-textured and textured surfaces lubricated with ISO VG 46: $v_{40} = 46 \text{ mm}^2/\text{s}$ and ISO VG 320: $v_{40} = 320 \text{ mm}^2/\text{s}$ ($F_N = 40 \text{ N}$).

5.2.2. Comparison between low viscosity (ISO VG 46) and medium viscosity (ISO VG 150) oil

Figure 5.5 shows the steady-state coefficient of friction for un-textured and textured surfaces lubricated with ISO VG 46 and ISO VG 150, for the six different sliding speeds. At low sliding speed from 0.03 m/s up to 0.1 m/s, the smooth surface showed lower coefficient of friction than all the textured surfaces and with the coefficient of friction increasing as the pattern area density increases. However, as we move towards higher sliding speeds from 0.1 up to 1 m/s an inversion occurred with the textured pattern with lower density (dashed orange line), showing lower coefficient of friction than the smooth surface (dashed blue line).

Again, the differences between the coefficient of friction for un-textured and textured discs at higher sliding speeds become smaller due to the increase in lubricant viscosity, resulting in increasing lubricant film thickness as sliding speed increases.

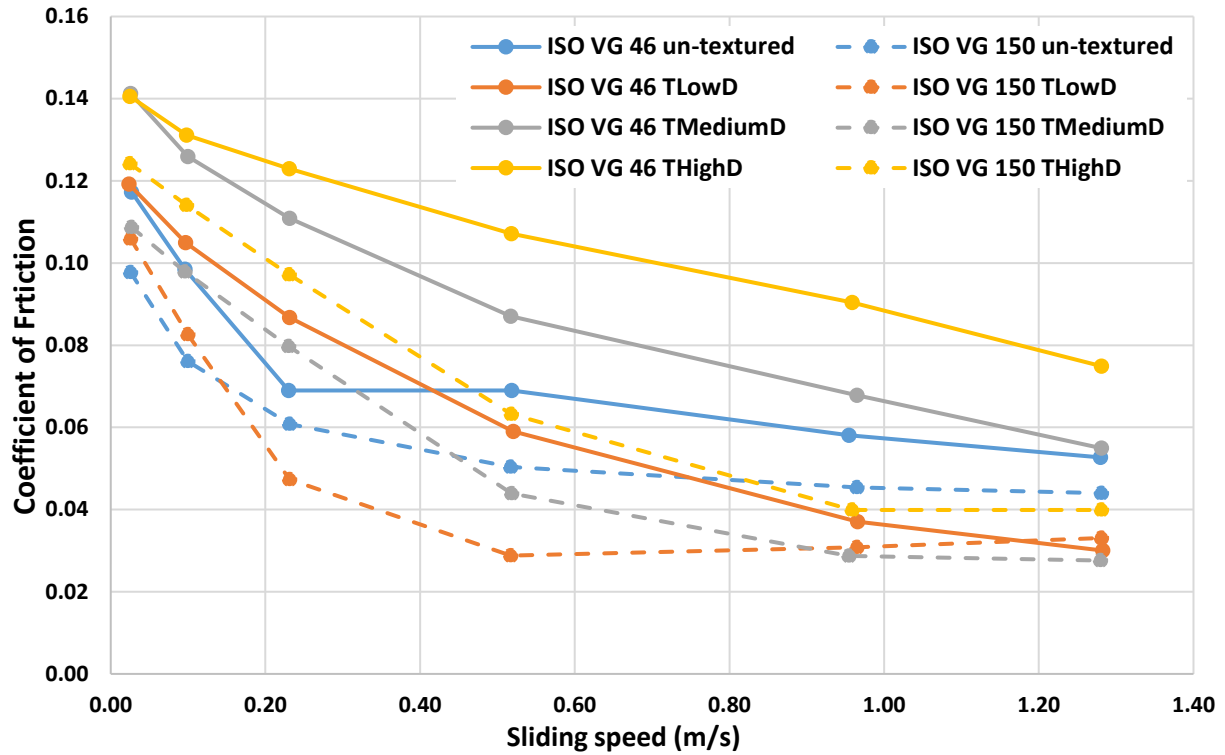


Figure 5.5. Variation in coefficient of friction with sliding speed for un-textured and textured surfaces lubricated with ISO VG 46: $\nu_{40} = 46 \text{ mm}^2/\text{s}$ and ISO VG 150: $\nu_{40} = 150 \text{ mm}^2/\text{s}$ ($F_N = 40 \text{ N}$).

5.3. Stribeck curves

Since we used three different lubricants ISO VG 46 (PAO8), ISO VG 320 and ISO VG 150 for the four different specimens tested (one un-textured and three textured). It is possible to build Stribeck curves by normalizing the six different sliding speeds (0.03, 0.1, 0.25, 0.5, 1.0 and 1.27 m/s) to the adimensional parameter sliding speed*viscosity/load. Figure 5.6 shows the Stribeck curve for the smooth sample where is possible to see the different data points obtained for the three different lubricant viscosities (blue, red and green data points).

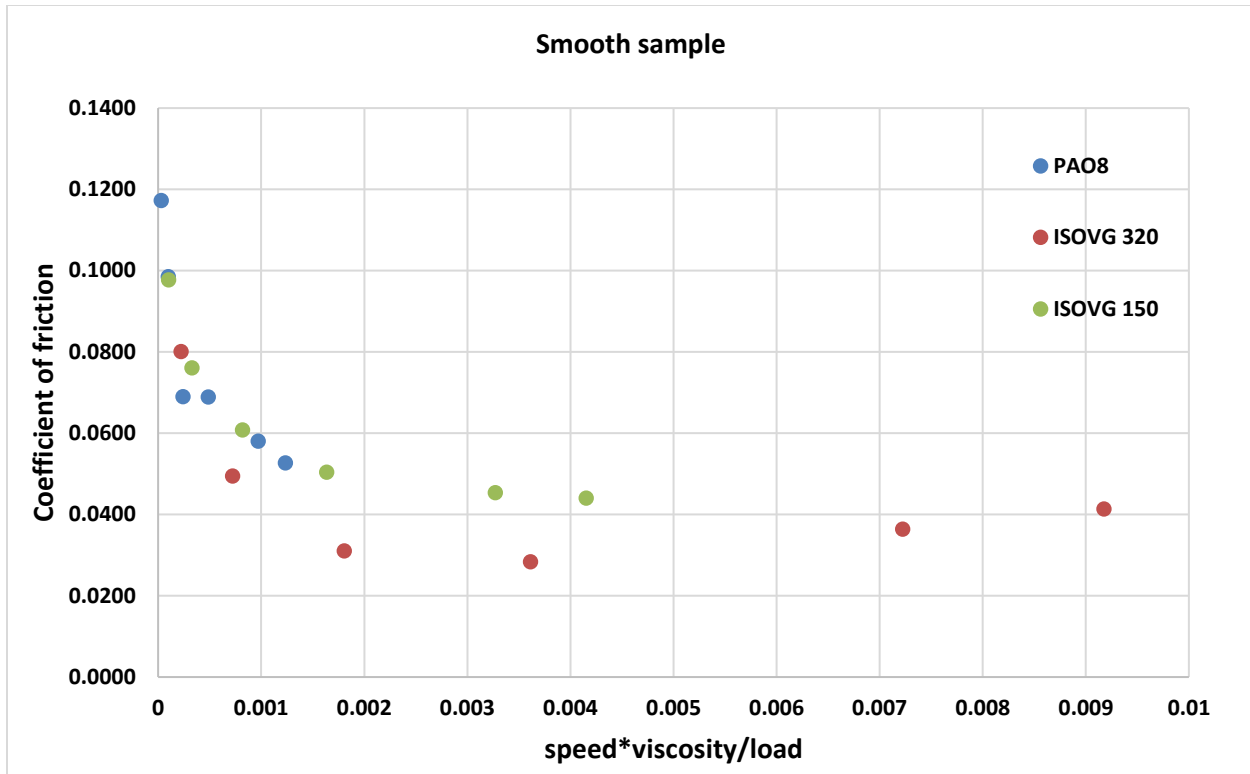


Figure 5.6. Variation in coefficient of friction with sliding speed*viscosity/load for un-textured surface lubricated with ISO VG 46: $\nu_{40} = 46 \text{ mm}^2/\text{s}$ (PAO8), ISO VG 150: $\nu_{40} = 150 \text{ mm}^2/\text{s}$ and ISO VG 320: $\nu_{40} = 320 \text{ mm}^2/\text{s}$ ($F_N = 40 \text{ N}$).

The same procedure was repeated to obtain Stribeck curves for textured specimens with low, medium and high textured density. In this way, all set of data points were joined together on one figure to get four stribeck curves for untextured and textured discs. Figure 5.7 shows data points for Stribeck curves for all specimens, both textured and un-textured, lubricated with three different lubricants ISO VG 46: $\nu_{40} = 46 \text{ mm}^2/\text{s}$, ISO VG 150: $\nu_{40} = 150 \text{ mm}^2/\text{s}$ and ISO VG 320: $\nu_{40} = 320 \text{ mm}^2/\text{s}$ ($F_N = 40 \text{ N}$). The spread of data points is due to the use of different lubricant viscosities. Average Stribeck curves were obtained from these points and are shown in Figure 5.8. It can be seen in Figure 5.8 that lower density textured sample showed beneficial effects in range of medium oil viscosity (ISOVG 150).

The relation sliding speed*viscosity/ load in range from 0.0005 to 0.0035 shows beneficial effects of using texturing. So, beneficial effect of texturing, here is only for using low pattern

area density. The Figure 5.7 can be divided in three regions. Firstly, by using ISO VG 46, no effect of texturing was seen (in regions from 0 to 0.0005), with coefficient of friction increasing as textured density increases. Secondly, by using medium density oil ISOVG 150 (in regions from 0.0005 to 0.0035), lower density textured disc showed the lowest values of coefficient of friction in comparison to smooth and other textured specimens. Medium density textured sample has coefficient of friction in between smooth specimen and high density texturized sample. Finally, by using high viscosity oil, ISO VG 320 (in region between 0.0035 and 0.01), texturing again showed no beneficial effects. Also, by increasing higher viscosity oil, a thick oil film is formed between sliding bodies and all texturized samples has almost same values of coefficient of friction in this region.

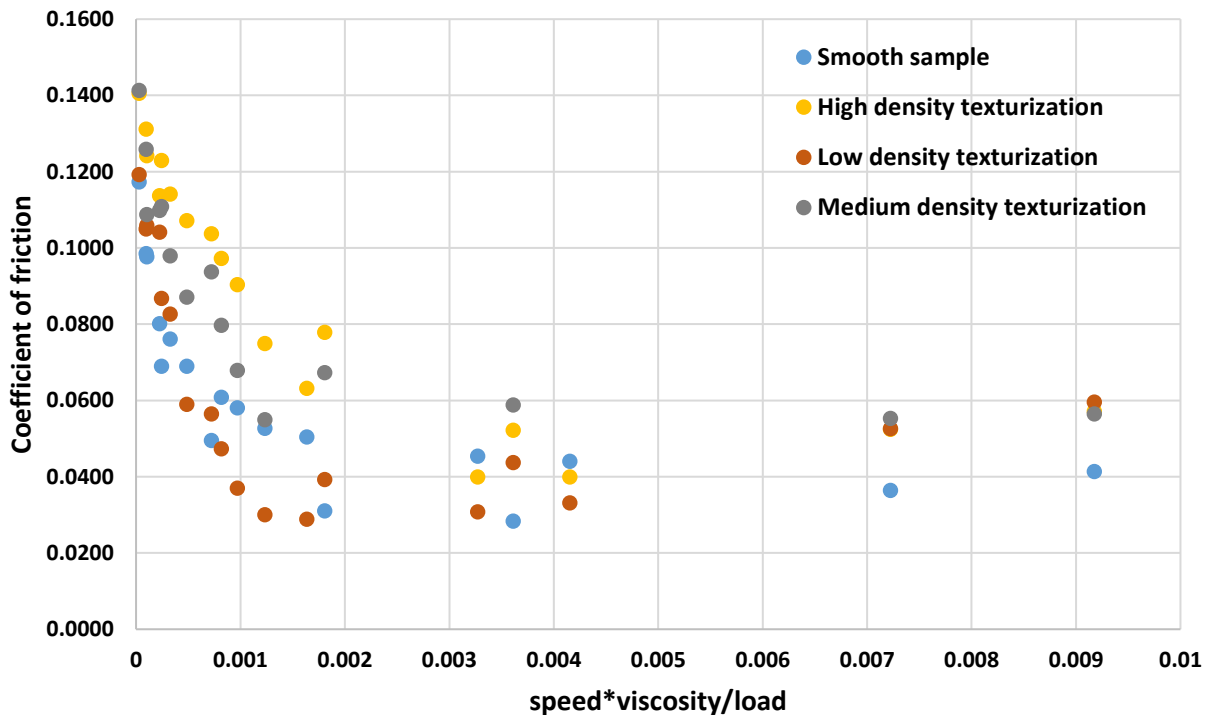


Figure 5.7. Variation in coefficient of friction with sliding speed*viscosity/load for textured and un-textured surfaces lubricated with ISO VG 46: $\nu_{40} = 46 \text{ mm}^2/\text{s}$ (PAO8), ISO VG 150: $\nu_{40} = 150 \text{ mm}^2/\text{s}$ and ISO VG 320: $\nu_{40} = 320 \text{ mm}^2/\text{s}$ ($F_N = 40 \text{ N}$).

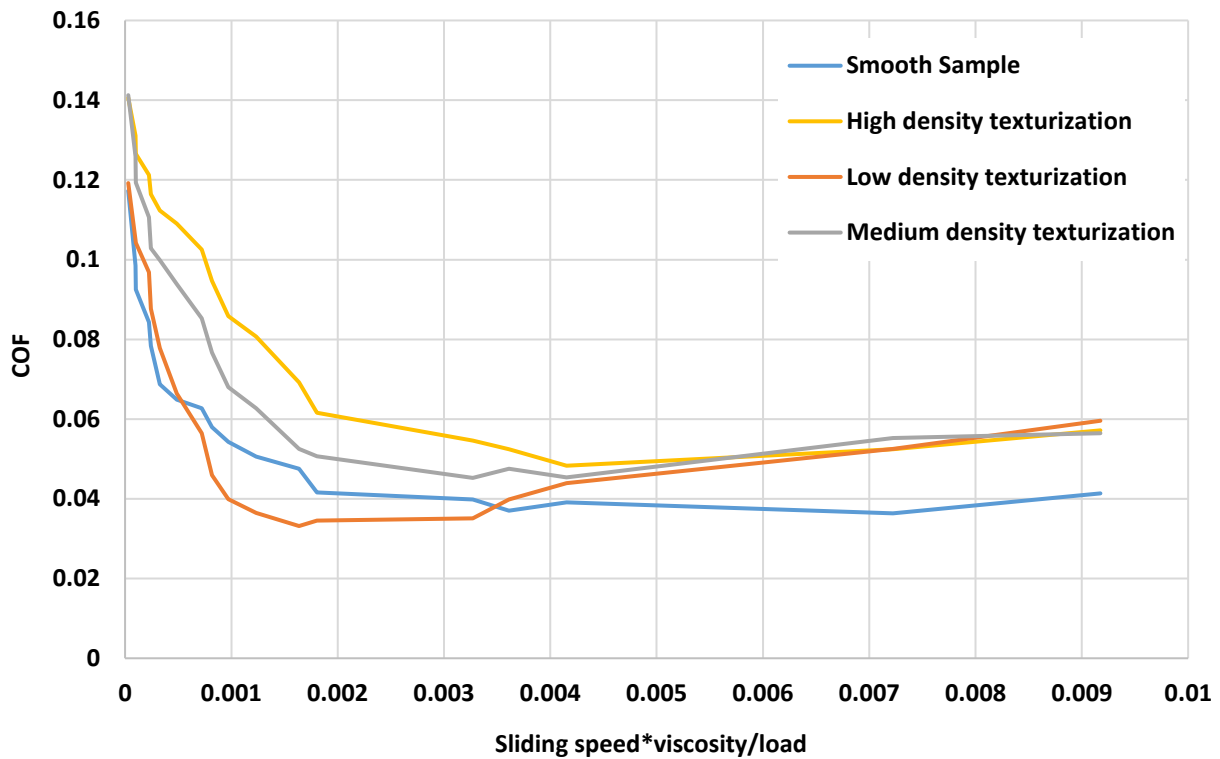


Figure 5.8. Average Stribeck curves for textured and un-textured surfaces lubricated with ISO VG 46: $\nu_{40} = 46 \text{ mm}^2/\text{s}$ (PAO8), ISO VG 150: $\nu_{40} = 150 \text{ mm}^2/\text{s}$ and ISO VG 320: $\nu_{40} = 320 \text{ mm}^2/\text{s}$ ($F_N = 40 \text{ N}$).

5.4. Effect of sliding velocity and lubricant viscosity on transitions in lubrication regimes

Table 5.1 shows the calculated values for the λ ratio of the film thickness to the composite surface roughness) for the three different lubricant viscosities. As long as the λ ratio is greater than unity the film thickness exceeds the mean surface roughness and severe wear is minimized. When λ is less than one as observed for PAO8 at 0.03 m/s sliding speed, the film thickness is smaller than the asperity height and the boundary lubrication regime exists. When λ becomes greater than five, values indicated by dark blue in the table, the highest asperities will no longer contact and ideal full film or hydrodynamic lubrication exists. In between these two extremes mixed lubrication regime exists, because λ is greater than one and less than five and values are indicated by blue in the table.

Table 5.1. Specific film thickness (λ) values for six different sliding speeds and three different lubricant viscosities, showing the variation in the lubrication regime (boundary - light blue: $\lambda < 1$; mixed - blue: $1 < \lambda < 5$ and hydrodynamic - dark blue $\lambda > 5$).

Sliding speed (m/s)	0.03	0.1	0.25	0.5	1.0	1.27
PAO8	0.7	1.6	3.0	4.7	7.6	9.0
h_0 (m)	3.37E-08	7.64E-08	1.42E-07	2.28E-07	3.65E-07	4.30E-07
ISO VG 150	1.6	3.6	6.8	10.8	17.4	20.4
h_0 (m)	7.69E-08	1.74E-07	3.25E-07	5.21E-07	8.34E-07	9.82E-07
ISO VG 320	2.7	6.2	11.6	18.6	29.8	35.0
h_0 (m)	1.32E-07	2.99E-07	5.57E-07	8.93E-07	1.43E-06	1.68E-06

The effect of increasing the lubricant viscosity contributes to that the transition from a boundary, mixed and hydrodynamic lubrication regime occur at lower speeds. It can be seen in Table 5.1 for PAO8, all the lubrication regimes exist within these range of sliding speeds. The transition from boundary to mixed lubrication occurs between 0.03 and 0.1 m/s, while from mixed to hydrodynamic lubrication, the transition occurred between 0.5 and 1.0 m/s. For higher viscosity oil, ISO VG 320 only mixed and hydrodynamic lubrication are found with the transition from mixed to hydrodynamic lubrication occurring between 0.03 and 0.1 m/s. Minimum film thickness is also given in the Table 5.1. It can be notice that minimum film thickness increases with increasing sliding speed for each oil and for higher viscosity oil ISO VG 320 oil film thickness has the highest values among all lubricants.

6. Conclusions

- This work showed the role played by surface texturing in both hydrodynamic and boundary/mixed regime and its potential to reduce friction. This study focused on textured patterns of grooves with three different pattern area densities. The effect of sliding speed and lubricant viscosity on friction, was studied and compared with un-textured case.
- Contact conditions were found to be an important factor in terms of tribological behaviour of textured surfaces. One of the main parameters governing friction behaviour is the contact pressure. The real pressure value can indeed be higher than theoretical calculated (0.04GPa). In textured specimens, real contact area is only a part of the contact surface, due to the higher textured density.
- Tribological behaviour of textured surfaces was found to greatly depend on the textured pattern density as well as on the dominant lubrication mode (operating conditions).
- For lower viscosity oil (ISO VG 46) the beneficial effect of micro-grooves becomes larger with a decrease in groove density as well as for higher sliding speeds (0.5, 1.0 and 1.27 m/s).
- For medium viscosity oil (ISO VG 150), all the textured specimens showed lower coefficient of friction than smooth specimen for higher sliding speeds (1.0 and 1.27 m/s).
- For higher viscosity oil (ISO VG 320), textured specimens did not show any beneficial effect in reduction friction.
- For higher viscosity oils (e.g.: ISO VG 320), the transition from boundary to mixed and to hydrodynamic lubrication regimes occurred at lower speeds. Additionally, the slope in the hydrodynamic lubrication increases with increasing viscosity.
- Average Stribeck curves, considering the three different lubricant viscosities and normalizing the sliding speed to the adimensional parameter sliding speed*viscosity/load showed that the beneficial effect of surface texturing occurred at the mixed lubrication regime.

Bibliography

- [1] Hsu, S. Implementing Agreement for a Program of Research and Development on Advanced Materials for Transportation Applications. IEA, Strategic Plan. Washington : s.n., 2008.
- [2] Etsion, I. Improving tribological performance of mechanical components by laser surface texturing. *Tribol. Lett.* 2004, Vol. 17, pp. 733-737.
- [3] Suh, N.P., Mosleh, M. and Howard, P.S. Control of friction. *Wear.* 1994, Vol. 175, pp. 151-158.
- [4] Hu, Z.M. and Dean, T.A. A study of surface topography, friction and lubricants in metal forming. *Int. Journal of Machine Tools & Manufacture.* 2000, Vol. 40, pp. 1637-1649.
- [5] Svahn, F., Kassman-Rudolphi, A. and Wallen, E. The influence of surface roughness on friction and wear of machine element coatings. *Wear.* 2003, Vol. 254, pp. 1092-1098.
- [6] Tayebi, N. and Polycarpou, A.A. Modeling the effect of skewness and kurtosis on the static friction coefficient of rough surfaces. *Tribology International.* 2004, Vol. 37, pp. 491-505.
- [7] Santner, E., et al. Effects of friction on topography and vice versa. *Wear.* 2006, Vol. 261, pp. 101-106.
- [8] Meine, K., et al. The influence of roughness on friction: Part I: The influence of a single step. *Wear.* 2002, Vol. 253, pp. 725-732.
- [9] Meine, K., et al. The influence of roughness on friction: Part II: The influence of multiple steps. *Wear.* 2002, Vol. 253, pp. 733-738.
- [10] Wang, W., et al. Effect of surface roughness parameters on mixed lubrication characteristics. *Tribology International.* 2006, Vol. 39, pp. 522-527.
- [11] Poon, C. Y. and Bhushan, B. Comparison of surface roughness measurements by stylus profiler, AFM and non-contact optical profiler. *wear.* 1995, Vol. 190, pp. 76-88.
- [12] Pettersson, U. and Jacobson, S. Friction and wear properties of micro textured DLC coated surfaces in boundary lubricated sliding. *Tribol. Lett.* 2004, Vol. 17, pp. 553-559.
- [13] Y. Kligerman, I. E. (July 2005). Improving Tribological Performance of Piston Rings by Partial Surface Texturing. 1-7.
- [14] Yuankai Zhou, H. Z. (n.d.). Influence of surface roughness on the friction property of textured surface. *Advances in mechanical engineering*, 1-9.

- [15] Gualtieri, E. (2004). Improving tribological properties of steels by surface texturing and coating. PhD courses in physics.
- [16] Ramesh, A. (2012). Friction characteristics of microtextured surfaces under hydrodynamic lubrication. Thesis
- [17] Daniela G Coblas, Aurelian Fatu, Abdelghani Maoui, Mohamed Hajjam. “Manufacturing textured surfaces: State of art and recent developments”: Journal of Engineering Tribology, July 10, 2014
- [18] Hsu, S. (2008). Integrated Surface Engineering for Improving Energy Efficiency. NTEL.
- [19] Halperin, I. E. (2008). A Laser Surface Textured Hydrostatic Mechanical Seal. Tribology Transactions, 1-6.
- [20] Kligerman, Y. (2001). Analysis of Hydrodynamic effects in surface textured circumferential gas seal. STLE, 472-478.
- [21] Chin Y. Poon, B. B. (1994). Comparison of surface roughness measurements by stylus profiler, AFM and non-contact optical profiler. Wear.
- [22] J. Oksanen, T. H. (2012). Tribological properties of laser textured and DLC coated surfaces with solid lubricants. 10-14.
- [23] (Blau, Use of Textured Surfaces to Mitigate Sliding Friction and Wear of Lubricated and Non Lubricated contacts, 2012)
- [24] Krishan Kumar Gupta, R. K. (2013). Study on Effect of Surface Texture on the Performance of Hydrodynamic Journal Bearing. International Journal of Engineering and Advanced Technology (IJEAT).
- [25] Wang X, Kato, K., Adachi K. and Aizawa K., “The effect of laser texturing of SiC surface on the critical load for the transition of water lubrication mode from hydrodynamic to mixed”. Tribology International 34, 2001, 703–711.
- [26] Wakuda M., Yamauchi Y., Kanzaki S., Yasuda Y., “Effect of surface texturing on friction reduction between ceramic and steel materials under lubricated sliding contact”. Wear 254, 2003, 356–363.
- [27] Andriy Kovalchenko , Oyelayo Ajayia, Ali Erdemira , George Fenskea , Izhak Etsionb. “The effect of laser surface texturing on transitions in lubrication regimes during unidirectional sliding contact”: Tribology International 38 (2005) 219–225

- [28] A. M. Kovalchenko. “State of investigations of surface texturing for tribological characteristics improvement of the friction units (A Review)”: Institute for Problems of Materials Science National Academy of Science of Ukraine: УДК 621.891:531.43
- [29] Ronen A., Etsion I. and Kligerman Y. (2001) Friction-reducing surface-texturing in reciprocating automotive components, *Tribology Transactions*, Vol. 44, pp. 359–366.
- [30] Kligerman Y., Etsion I. and Shinkarenko A. (2005) Improving tribological performance of piston rings by partial surface texturing, *Journal of Tribology-Transactions of the ASME*, Vol. 127, pp. 632–638.
- [31] Ryk G., Kligerman Y., Etsion I. and Shinkarenko A. (2005) Experimental investigation of partial laser surface texturing for piston-ring friction reduction, *Tribology Transactions*, Vol. 48, pp. 583–588.
- [32] Ryk G. and Etsion I. (2006) Testing piston rings with partial laser surface texturing for friction reduction, *Wear*, Vol. 261, pp. 792–796.
- [33] Etsion I., Halperin G. and Becker E. (2006) The effect of various surface treatments on piston ring scuffing resistance, *Wear*, Vol. 261, pp. 785–791.
- [34] Ryk, G., Kligerman, Y., and Etsion, I., Experimental Investigation of Laser Surface Texturing for Reciprocating Automotive Components, *STLE Tribology Transactions*, Vol. 45, No. 4, 2002, pp. 444-449.
- [35] Vijay K. Patel, Hiren P.Patel, Hitesh J. Yadav, Prof. V.R.Patel. “Experimental investigation of laser surface texturing on piston rings for friction reduction and improving fuel efficiency-a review study, *International Journal of Advanced Engineering Technology*,1-5.
- [36] Patel Kalpeshkumar P. (2015). Effect of different parameter of LST: an overview. *IJEDR*, 1-5.
- [37] Narita, K. (2012). Tribological Properties of Metal V-Belt Type CVT Lubricant. *Advances in Tribology*, 1-8.
- [38] Antoszewski Bogdan. Mechanical Seals With Sliding Surface Texture – Model Fluid Flow and Some Aspects of the Laser Forming of the Texture: *Procedia Engineering* 39 (2012) 51 – 62
- [39] Etsion I., Halperin G., Brizmer V. and Kligerman Y. (2004) Experimental investigation of laser surface textured parallel thrust bearings, *Tribology Letters*, Vol. 17, pp. 295–300.

- [40] Marian V. G., Kilian M. and Scholz W. (2007) Theoretical and experimental analysis of a partially textured thrust bearing with square dimples, Proceedings of the Institution of Mechanical Engineers Part J-Journal of Engineering Tribology, Vol. 221, pp. 771–778.
- [41] Cupillard S., Glavatskih S. and Cervantes M. J. (2008) Computational fluid dynamics analysis of a journal bearing with surface texturing, Proceedings of the Institution of Mechanical Engineers Part J-Journal of Engineering Tribology, Vol. 222, pp. 97–107.
- [42] Glavatskih S. B., McCarthy D. M. C. and Sherrington I. (2005) Hydrodynamic performance of a thrust bearing with micropatterned pads, Tribology Transactions, Vol. 48, pp. 492–498.
- [43] Lu X. B. and Khonsari M. M. (2007) An experimental investigation of dimple effect on the Stribeck curve of journal bearings, Tribology Letters, Vol. 27, pp. 169–176.
- [44] Borghi A., Gualtieri E., Marchetto D., Moretti L. and Valeri S. (2008) Tribological effects of surface texturing on nitriding steel for highperformance engine applications, Wear, Vol. 265, pp. 1046–1051.
- [45] Wan Y. and Xiong D. S. (2007) Influence of laser surface texturing on tribological performance of mechanical components, Journal of Central South University of Technology, Vol. 14, pp. 79–82.
- [46] Rashwan, O. (2013). Micro Surface Texturing for Friction Control. Electronic Theses and Dissertations, 3-196.
- [47] Mihir Kumar Ghosh, Bankim Chandra Majumdar, Mihir Sarangi. Theory of lubrication, Tata McGrawhill education Private Limited (December 14, 2012), PP (3-4).
- [48] Kovalchenko A., Ajayi O., Erdemir A., Fenske G. and Etsion I. (2004) The effect of laser texturing of steel surfaces and speed-load parameters on the transition of lubrication regime from boundary to hydrodynamic, Tribology Transactions, Vol. 47, pp. 299-307.
- [49] Hsu, S. M. Surface Texturing: Principles and Design. National Institute of Standards & Technology. Maryland, USA : s.n., 2006
- [50] Stephens, R. and L., Siripuram. Effect of Deterministic Asperity Geometry on Hydrodynamic Lubrication. ASME Journal of Tribology.2004, Vol.126, pp. 527-534
- [51] Etsion, I., Kligerman, Y. and Halperin, G. STLE Tribol. Trans. 1999, Vol. 42, p. 511.
- [52] Pradeep Kumar C, Pradeep L. Menezes, and Satish V. Kailas. “Role of surface texture on friction and wear under boundary lubricated conditions”:International Conference on Industrial Tribology – 2006

- [53] Peter M. Thompson, William R. Jones, Jr., Mark J. Jansen, Joseph M. Prah. "The Effect of Sliding Speed on Film Thickness and Pressure Supporting Ability of a Point Contact Under Zero Entrainment . Velocity Conditions": Society of Tribologists and Lubrication Engineers Orlando, Florida, May 20-24, 2001
- [54] Ing. Fadi Ali. "Effect of surface texturing on friction and film thickness under starved lubrication conditions": Brno university of technology, ISBN 80-214- ISSN 1213-4198.
- [55] Morris, Nicholas J., Rahnejat, Homer, Rahmani, Ramin. "Tribology of partial pad journal bearings with textured surfaces": The Austrian Tribology Society, 2011.
- [56] B.J. Hamrock and D. Dowson, Ball Bearing Lubrication, The Elastohydrodynamics of Elliptical Contacts John Willey & Sons, 1981.
- [57] B.J. Hamrock and D. Dowson, Isothermal Elastohydrodynamic Lubrication of Point Contacts, Part III – Fully Flooded Results, Transactions ASME, Journal of Lubrication Technology, Vol. 99, 1977, pp. 264-276.
- [58] L.B. Sargent Jr, Pressure-Viscosity Coefficients of Liquid Lubricants, ASLE Transactions, Vol. 26, 1983, pp. 1-10.

